Contrib Mineral Petrol (2007) 153:533–555
DOI 10.1007/s00410-006-0161-9

ORIGINAL PAPER

Prograde and retrograde history of the Junction School eclogite, California, and an evaluation of garnet–phengite–clinopyroxene thermobarometry

F. Zeb Page · Lora S. Armstrong · Eric J. Essene · Samuel B. Mukasa

Received: 18 May 2006 / Accepted: 6 November 2006 / Published online: 8 December 2006

Abstract Quantitative thermobarometry of inclusions in zoned garnet from a Franciscan eclogite block record a counter-clockwise *P–T* path from blueschist to eclogite and back. Garnet retains prograde zoning from inclusion-rich $Alm_{52}Grs_{30}Pyp_{6}Sps_{12}$ cores to inclusion-poor $Alm_{62}Grs_{25}Pyp_{12}Sps_{1}$ mantles, with overgrowths of highly variable composition. Barometry using the Waters–Martin version of the garnet–phengite–omphacite thermobarometer yields conditions of 7–15 kbar, 400–500°C (garnet cores), 18–22 kbar, ~550°C (mantles), and 10–14 kbar, 350–450°C (overgrowths), in agreement with clinozoisite–sphene–rutile–garnet–quartz barometry. These pressures are ~10–15 kbar less than those obtained using more recent, fully thermodynamic calibrations of the phengite–omphacite–garnet thermobarometer. Low early temperatures suggest that the block was subducted in a thermally mature subduction zone and not at the inception of subduction when prograde temperature is expected to be higher. Franciscan high-grade blocks likely represent crust subducted throughout the history of this convergent margin, rather than only at the inception of the subduction zone.

Communicated by Jochen Hoefs.

F. Z. Page · L. S. Armstrong · E. J. Essene · S. B. Mukasa
Department of Geological Sciences,
University of Michigan, 2534 C.C. Little Building,
Ann Arbor, MI 48109-1005, USA

F. Z. Page (✉)
Department of Geology and Geophysics,
University of Wisconsin—Madison,
1215 W. Dayton St., Madison, WI 53706, USA
e-mail: zeb@geology.wisc.edu

Present Address:
L. S. Armstrong
Department of Earth Sciences,
University of Bristol, Wills Memorial Building,
Queen's Road, Bristol BS8 1RJ, UK

Introduction

The construction of pressure–temperature (*P–T*) paths that document the metamorphic history of eclogites can yield dramatic insight into the conditions and processes that take place within subduction zones. However, thermobarometry of eclogites has long been understood to be fraught with difficulty and uncertainty. Most eclogite is fully recrystallized during metamorphism into the characteristic high-variance assemblage of garnet + omphacite ± quartz ± rutile, and the high variance hampers useful barometers in many eclogites (Essene 1989). Until recently, barometry of eclogite was typically limited to a pressure minimum from the reaction albite = jadeite + quartz (Holland 1980), and thermometry was obtained from the Fe^{2+}-Mg exchange between garnet and clinopyroxene (e.g., Ravna 2000). Even this straightforward approach has pitfalls, however. The effect of cation ordering in omphacite (Essene 1982) and the presence of Fe^{3+} versus Ca-Eskola (CaEs) molecule in eclogitic clinopyroxene cannot be measured directly using standard electron-beam analytical techniques (Proyer et al. 2004; Page et al. 2005). If the dilutions caused by Fe^{3+} and CaEs are not carefully evaluated, both conventional thermometry and barometry will include systematic errors (e.g., Ravna and Paquin 2003; Proyer et al. 2004).

More recently, quantitative thermobarometers have been developed based on equilibria involving the accessory phases in eclogites such as phengitic muscovite (Waters and Martin 1993), zoisite/clinozoisite (Manning and Bohlen 1991; Page et al. 2003), sanidine (Tropper et al. 1999), or kyanite (Sharp et al. 1992). These methods have at last allowed quantitative measurement of eclogite facies pressure, but each reaction assemblage represents only one point on a *P–T* loop; it is often difficult to obtain data that more fully constrains the *P–T* path of eclogites.

The matrix minerals of eclogite are strongly overprinted during decompression and retrograde metamorphism (e.g., Carswell 1990), and many eclogite *P–T* paths consist of a rather uncertain maximum, followed by a better-established decompression path. One approach to the reconstruction of prograde conditions has been through the use of inclusions in garnet. Krogh (1982) pioneered this procedure using chemical zonation in host garnet as a context for the minerals entrapped during garnet growth. Despite the power of this technique, it has seldom been put to use in eclogite studies. Even when inclusions in garnets were being considered, evaluation of prograde *P–T* conditions was generally only qualitative (cf. Page et al. 2003 for a brief review). Dramatic improvements in the past twenty years in backscattered electron imaging (BSE) and thermobarometry using self-consistent data sets and newly calibrated equilibria make this approach all the more powerful.

Massonne (1995) applied quantitative garnet–omphacite–phengite barometry to inclusions and matrix minerals in a Franciscan eclogite from the Junction School locality, obtaining *P* in excess of 28 kbar at 500°C. These conditions are well within the stability field of coesite, implying subduction of eclogite to a much greater depth than ever before considered in this region. In this study, a detailed examination is made of the matrix and inclusion mineralogy of the Junction School eclogite block. In an effort to constrain a detailed *P–T* path, the method pioneered by Krogh (1982) is coupled with the most recent quantitative thermobarometry. By using multiple thermobarometers we tested both the existing qualitative *P–T* paths from blocks in the Franciscan and the new empirically calibrated eclogite barometers.

Geologic context

The Franciscan complex of central and northern California has long been recognized to be a fossil subduction zone accretionary wedge (Bailey et al. 1964; Ernst et al. 1970). Wakabayashi (1999) recently reviewed the literature on the Franciscan complex. Eclogite, garnet hornblendite (commonly referred to as amphibolite or garnet amphibolite despite the lack of plagioclase), and coarse-grained, garnet-bearing blueschist are found as 1–300 m blocks (e.g., Coleman and Lanphere 1971) in a matrix of low-grade metasedimentary rocks and/or serpentinites (Bailey et al. 1964; Ernst et al. 1970; Coleman 1980). Although the high-grade blocks constitute a very small percentage of their host formation, they have attracted much study over the last century, because of their striking mineralogy, unusual field relations as tectonic blocks in a lower-grade metamorphic matrix, and poorly understood exhumation mechanisms.

The high-grade blocks were collectively referred to as ''glaucophane schists'' from the first description of glaucophane in California (Becker 1888), and that appellation remained in use until the second half of the 20th Century. Although many blocks are found as float and within the Franciscan mélange, they are almost always found in proximity to, or in contact with serpentinites; often the blocks are encased in metasomatic selvages that suggest a reaction relationship with ultramafic rocks (Ransome 1894; Essene et al. 1965; Coleman 1980).

A key textural feature of the high-grade blocks—such as glaucophane, lawsonite, albite, and chlorite being texturally late in many blocks was recognized in the first descriptions of glaucophane schists in the Franciscan Group (e.g., Palache 1894; Ransome 1895; Holway 1904). This textural analysis gave rise to general acceptance of a pervasively late blueschist-facies overprint on both eclogite (Brothers 1954; Borg 1956; Bloxam 1959; Coleman and Lanphere 1971) and hornblendite (Hermes 1973). Although it is tempting to correlate that overprint with the regional blueschist facies metamorphism that is often seen in the adjacent country rocks, mainly basalt and greywacke, that correlation is still in need of confirmation with the use of robust thermochronometers.

More recent and detailed petrographic studies have begun to elucidate the retrograde path of the high-grade blocks and their prograde history. Essene (1967) identified both omphacite veins and zones that overprinted garnet amphibolite blocks in the Panoche Valley. Moore (1984) recognized three distinct late high *P*/*T* stages in high-grade blocks from the Diablo Range, California. Moore and Blake (1989) recognized both eclogite and blueschist overprints on hornblendite blocks from the Franciscan. They interpreted these textures as evidence that some hornblendite blocks are remnants of earlier metamorphism or samples from the

prograde path of higher-pressure rocks. Wakabayashi (1990) described similar overprinting in hornblende eclogite from Tiburon, California, and constructed a counter-clockwise *P–T* path in which garnet hornblendite (~650°C, 9 kbar) was cooled and compressed to form eclogite (~550°C, >11 kbar) and then was further cooled and decompressed to form blueschist (~350°C, >8 kbar). Qualitative *P–T* estimates on inclusions in garnet from eclogite provide further support for an amphibolite or blueschist facies precursor and a counter-clockwise *P–T* path. Krogh et al. (1994) and Oh and Liou (1990) described inclusions of barroisitic and actinolitic amphibole, epidote, omphacite and sphene that were entrapped during prograde growth of chemically zoned garnet in eclogite and blueschist blocks from Ward Creek and Jenner, California. These workers also proposed a counter-clockwise *P–T* path based on estimates from a generalized petrogenetic grid of the metamorphic facies and limited application of quantitative calculations.

Isotopic dating of Franciscan metamorphic rocks began in the early 1960s and has made use of a variety of methods. The most recent work has employed the $^{40}Ar/^{39}Ar$ and Lu–Hf systems to establish two groups of ages in the high-grade blocks. The $^{40}Ar/^{39}Ar$ hornblende ages of hornblendites and Lu–Hf ages of hornblendites and eclogites range from ~155 to ~170 Ma (Lanphere et al. 1978; Ross and Sharp 1988; Wakabayashi and Deino 1989; Catlos and Sorensen 2003; Anczkiewicz et al. 2004). The $^{40}Ar/^{39}Ar$ ages of texturally late phengite in the Franciscan and Lu–Hf ages of garnet blueschist cluster around ~140–145 Ma (Sharp et al. 1987; Wakabayashi and Deino 1989; Catlos and Sorensen 2003; Anczkiewicz et al. 2004).

Glaucophane schists were first described in the vicinity of Healdsburg, California, by Nutter and Barber (1902), including a garnet–actinolite (possibly a misidentification of omphacite) rock. Holway (1904) first identified eclogite in the Franciscan in the Berkeley Hills and suggested that Nutter and Barber's sample near Healdsburg was also an eclogite. The eclogite body in this study is located ~ 5 km SW of Healdsburg, California (Fig. 1), and it was first described in detail by Switzer (1945). A description and map of the blocks at this locality, traditionally referred to as the Junction School eclogite, was published by Borg (1956). The eponymous Junction School that was nearby the exposure has long since been dismantled. Coleman et al. (1965) included data from this eclogite in their general study of eclogites worldwide. Massonne (1995) applied garnet–phengite–clinopyroxene thermobarometry to this block obtaining pressures as high as 28–30 kbar, by far the highest pressures ever reported in the Franciscan.

Samples for this study were taken from a ~50 m^2 tectonic block, the largest block at this locality (on the east side of Mill Creek Rd., 38°35′42″N, 122°53′50″W), which is on private property requiring advance permission to sample. The contact of the block with the country rock is obscured, although, as with most high-grade metamorphic blocks of the Franciscan, serpentinite bodies are present in the immediate vicinity. It is unclear whether the eclogite was hosted by Franciscan greywacke, associated ultramafic rocks or mélange. Unlike many blocks in the Franciscan (e.g., Coleman 1980; Moore 1984; Krogh et al. 1994) the block does not have a distinct rind, nor does it have pervasive, late glaucophane throughout the outcrop. In hand-sample the eclogite consists dominantly of equigranular, small (≤ 1 mm) grains of clinopyroxene and garnet, with varying amounts of white mica and dark green chlorite and occasional glaucophane. The outcrop has a mottled appearance, darker patches containing a higher percentage of chlorite and mica and fractures and joints in the rock carrying abundant mica. Samples were selected to represent a continuum from the most pristine eclogite (lighter green, almost exclusively

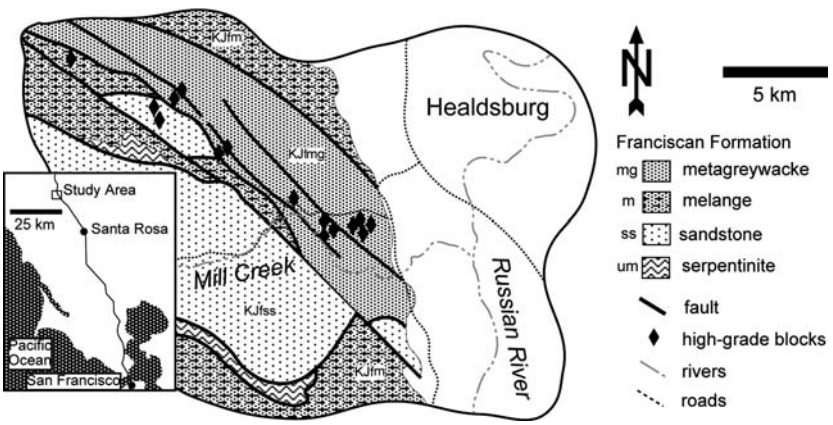

Fig. 1 Geologic sketch map of the vicinity of Healdsburg, California (after Gealey 1951)

garnet and clinopyroxene visible in hand sample) to the most heavily overprinted (darker green, dominantly garnet and clinopyroxene with more abundant white mica and chlorite). However, the most overprinted samples collected for this study contain fewer typical blueschist-facies minerals visible in hand-sample than the many other eclogite occurrences in California.

Petrography

The Junction School eclogite is a garnet–clinopyroxene rock consisting almost entirely of 100 μm–1 mm clinopyroxene and ~1 mm garnet grains (Fig. 2a, b). Garnet ranges from euhedral to strongly resorbed, chloritized and fractured on the thin section scale. Garnets from the Junction School body contain a rich population of inclusion phases including: quartz, clinopyroxene, epidote, sphene, rutile, phengite, calcite/aragonite, chalcopyrite, apatite and zircon (Figs. 2, 3). Matrix rutile crystals (10 μm–5 mm) are elongate, and partially to completely replaced by sphene.

Texturally late phases in the Junction School eclogite suggest abundant fluid flow and possibly open cavities. Quartz is found as inclusions in garnet (Figs. 2c, d, 4a), as an interstitial filling between matrix phases, and in some cases containing euhedral inclusions of other late phases. Figure 3a and 3b show quartz filling a region between matrix clinopyroxene. A euhedral clinopyroxene grain with a square cross-section is completely surrounded by the quartz. This clinopyroxene appears to have grown into a fluid-filled

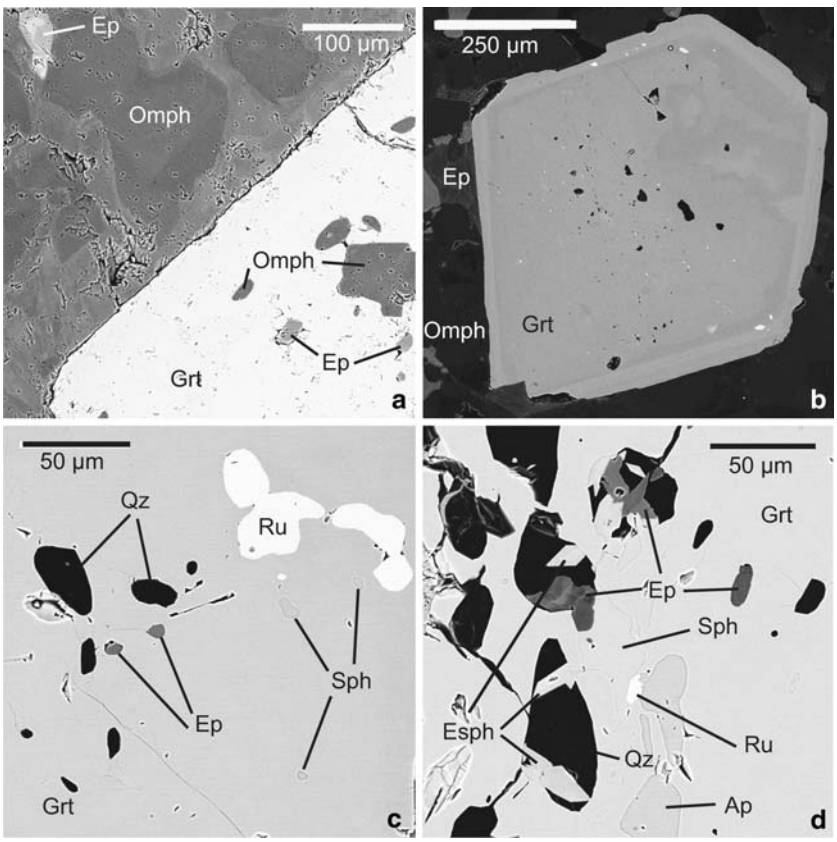

Fig. 2 Back-scattered electron (BSE) images. **a** Euhedral garnet with inclusions of epidote and omphacite. Matrix omphacite is chemically zoned with low-Z cores and high-Z Fe-rich rims. Late epidote is zoned in Sr and the rare earth elements. **b** Strongly zoned garnet in a more retrogressed sample. The *lower right portion* of the garnet core contains many small sphene inclusions. The *upper right core zone* shows evidence of strong resorption filled in with variably zoned garnet. A bright, high-Z, rim shows oscillatory zoning, and contains inclusions of rutile and zircon. **c** Inclusions in the core of garnet used for thermobarometry. These inclusions were used for *P–T* estimates because they are monomineralic, rounded, and do not appear to be aligned on cracks or healed fractures. The crack in the lower left does not extend a great distance, and was likely formed during the thin section manufacture. *d* Inclusions deemed unsuitable for thermobarometry. Inclusions of quartz, epidote, apatite, sphene, and rutile are polymineralic and aligned in a zone trending N–S in the garnet. Euhedral sphene crystals appear to have grown from the walls of Qz inclusions, which were possibly once filled with a high-pressure fluid. *Grt* garnet, *Omph* omphacite, *Ru* rutile, *Sph* sphene, *Phg* phengite, *Chl* chlorite, *Ep* epidote, *Qz* quartz, *Ap* apatite, *Esph* euhedral sphene, *Zr* zircon

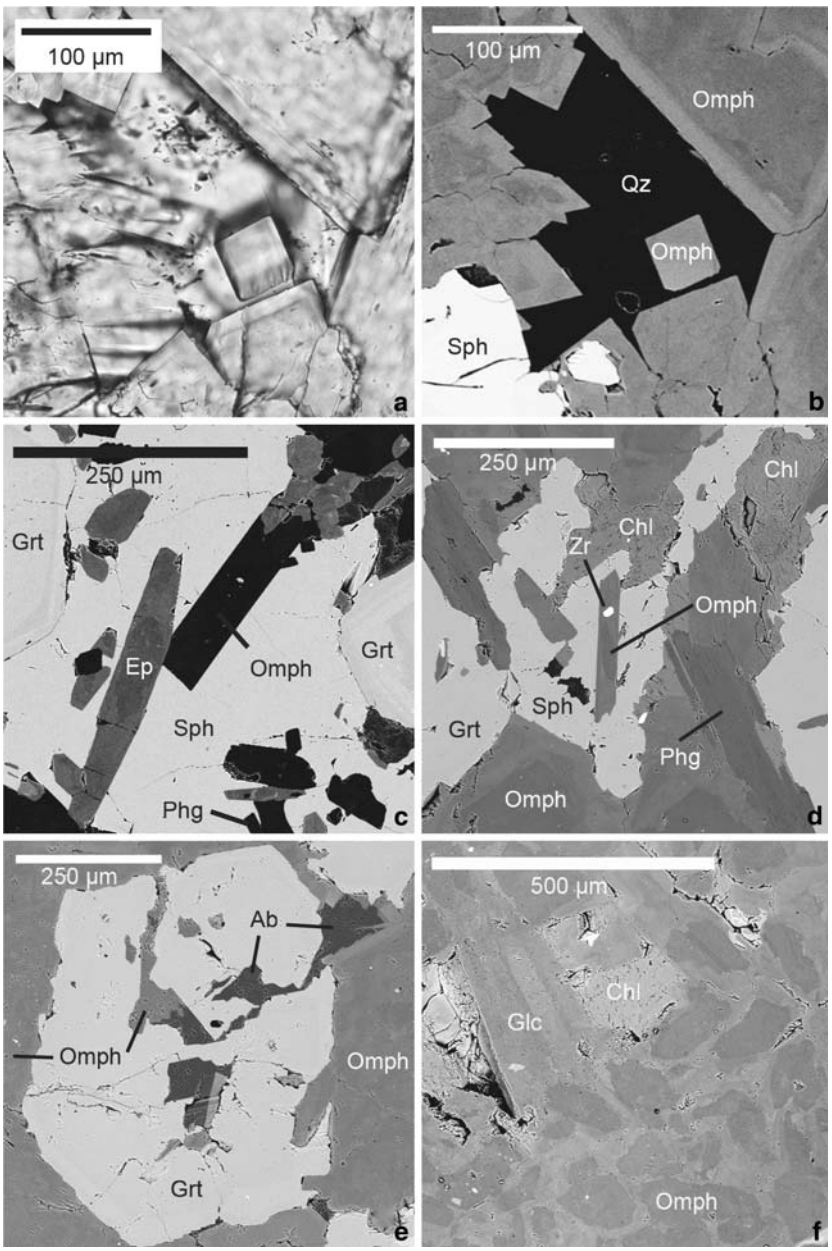

Fig. 3 Images of texturally late features. **a** Photomicrograph in plane polarized light of interstitial quartz with a euhedral omphacite inclusion. Phases are identified in (**b**). **b** BSE image of the same field of view. Omphacite has bright, high-Z rims. A euhedral omphacite crystal is surrounded by late quartz, and may have grown into a fluid-filled cavity now filled with quartz. **c** BSE of late sphene between strongly zoned garnets. Euhedral epidote, omphacite, and phengite are surrounded by sphene. **d** A BSE image of a similar texture to (**c**) with slightly rounded zircon in a late euhedral omphacite crystal surrounded by sphene. **e** BSE image of a corroded and fractured garnet. Late albite and omphacite veins cut garnet. Late albite is in contact with matrix omphacite rims. **f** BSE of rare late glaucophane and chlorite, possibly in equilibrium with omphacite rims. Abbreviations are as in Fig. 2, *Ab* albite

miariolitic cavity that was later filled in by quartz. Essene (1967) and Essene and Fyfe (1967) reported pyramidally terminated omphacite crystals growing into open vugs in Franciscan blocks. Some surrounding clinopyroxene grains have serrated crystal faces visible in transmitted light microscopy (Fig. 3a) through overlying quartz. Matrix quartz appears as a texturally late mineral, and may not be in equilibrium with the eclogite facies assemblage.

In more overprinted samples, matrix rutile is absent, and ~1 mm regions of sphene appear to fill zones between adjacent garnets. Many sphene crystals do not appear to be pseudomorphs of relict rutile, but contain euhedral inclusions of omphacite, epidote, phengite, and zircon (Fig. 3c, d). Rare albite is found as veins cutting garnet, and filling space between adjacent matrix clinopyroxene (Fig. 3e). Epidote is found as an inclusion in garnet (Fig. 2c), euhedral rods enclosed by late sphene (Fig. 3c), and anhedral grains on the margins of garnet (Fig. 3c). Phengite and chlorite are found on the margins of garnet as well, in some cases partially replacing resorbed garnet rims (Fig. 3d). Glaucophane is present as only a few grains in each thin section, and is texturally late, usually forming in conjunction with chlorite and possibly with omphacite rims (Fig. 3f).

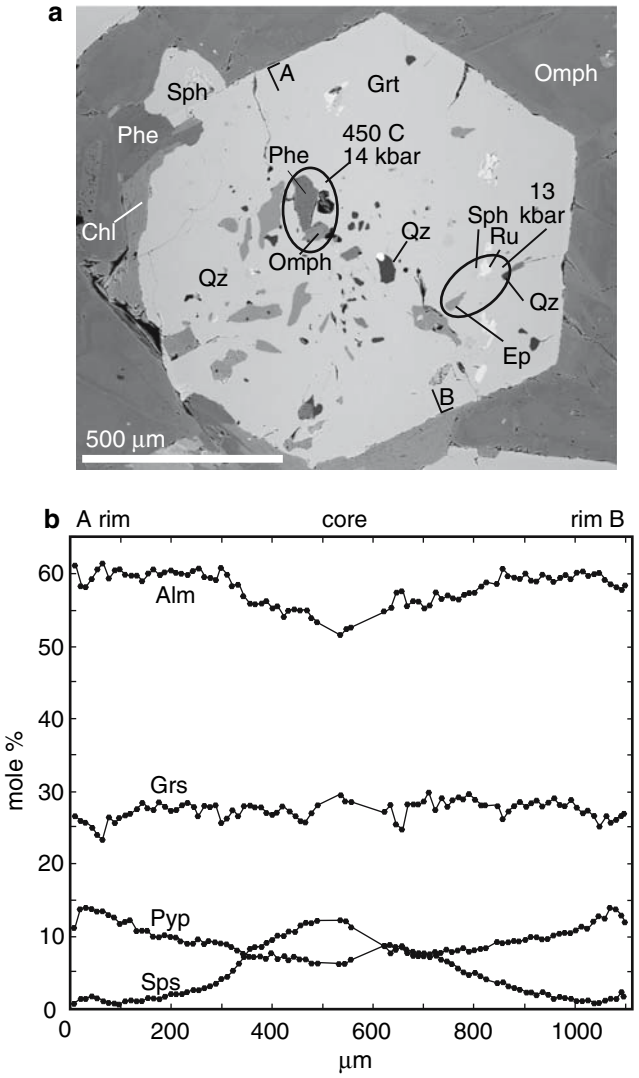

Fig. 4 BSE (**a**) and microprobe traverse (**b**) of a euhedral garnet from a minimally retrogressed sample. Inclusion assemblages used in thermobarometry are circled with their *P–T* conditions indicated. The traverse was performed between the ticks marked *A* and *B*. Mn decreases from core to rim in a bell-shaped profile with a small increase near the rim, but not at the edge of the crystal. Mg increases from core to rim, with a sudden decrease at the edge of the garnet, outside of the small Mn-rich annulus. Fe increases from core to rim, falling off in the region of the Mn annulus, then increasing at the outermost rim. Ca is rather constant, falling slightly from core to rim, possibly with a sudden dip associated with the Mn annulus

Mineral chemistry

Mineral chemistry was determined using the Cameca SX100 electron microprobe at the University of Michigan. Most minerals were analyzed in point beam mode at 15 kV and 10 nA, except for feldspar and mica, which were analyzed using a 15 kV, 4 nA beam rastered over 25 μm^2 to limit volatilization and elemental migration. Natural and synthetic silicate and oxide standards were used, and data were reduced using a Cameca PAP-type correction calculating oxygen by stochiometry.

Garnet

Garnet in the Junction School eclogite is dominantly almandine and is compositionally zoned (Table 1), but the degree and style of zoning varies both on the thin-section and outcrop scales. For most euhedral garnets in the less altered portions of the outcrop (Fig. 4), Mn decreases in a bell-shaped profile from spessartine-rich cores ($Alm_{52}Grs_{30}Pyp_6Sps_{12}$) to a mantle region low in Mn (Alm_{62} Grs_{25} Pyp_{12} Sps_1). As the Mn content decreases, both Fe and Mg increase and Ca remains constant over most of the grain with a slight decrease in the outer mantle. Approximately 50 µm from the edge of the garnet an annulus of increased Sps content is also marked by a decrease in Fe and Ca (Alm_{58} Grs_{23} Pyp_{15} Sps_4). At the outermost margin of the garnet, Fe and Ca rebound, whereas Mg and Mn fall again (Alm_{61} Grs_{27} $Pyp_{11}Sps_1$). The fine scale zoning in the garnet rims varies between garnets and even on different sides of a single garnet.

Garnet in thin sections with more evidence of retrogression also varies from euhedral to strongly resorbed. The zoning patterns in the rims of these garnets are similar to those described above, but are wider and more intense than the zoning observed in less overprinted samples. In high-contrast BSE images (Fig. 5a) the average atomic number (Z) of the garnet can be seen to decrease slowly in the core region of the garnet until there is a sharp decrease in Z approximately 50 µm from the rim. Quantitative traverses (Fig. 5b) show that the core region has a Mn-rich center ($Alm_{57}Grs_{27}Pyp_6Sps_{10}$) and slowly increasing Fe and Mg contents in the mantle region ($Alm_{60}Grs_{27}Pyp_{12}Sps_1$) similar to other garnets from less overprinted samples in this rock (Fig. 4). The discontinuity between the core and mantle regions and the low-Z annulus at its margin is undulatory and does not follow any crystal faces, suggesting a period of garnet dissolution. The low-Z annulus itself is characterized by a sharp increase in Mn and Mg content, coupled with a decrease in Fe ($Alm_{54}Grs_{29}Pyp_{14}Sps_4$, Fig. 5b), and fills in a portion of the resorbed garnet. The outer margin of the high-Mn (low-Z) annulus is another sharp compositional discontinuity leading to a high-Z annulus with a significant increase in Fe content and decrease in Mn and Ca content ($Alm_{64}Grs_{27}Pyp_9Sps_0$). This high-Fe region appears to have filled much of the remaining resorbed garnet, and shows renewed growth along crystal faces. Outside of the high-Z

Table 1 Representative garnet and clinopyroxene analyses

	Garnet Core Center	Garnet Core Edge (mantle)	Garnet Low-Z Annulus	Garnet High-Z Annulus	Garnet Rim		cpx Matrix Core	cpx Matrix Rim	cpx Inclusion Garnet core	cpx Inclusion Garnet mantle	cpx Inclusion Garnet rim
SiO_2	37.33	38.16	38.32	37.77	38.05	SiO_2	56.03	55.46	56.86	57.16	56.55
TiO_2	0.18	0.06	0.02	0.10	0.05	TiO_2	0.03	0.05	0.08	0.10	0.05
ZrO_2	n.d.	n.d.	0.01	0.01	0.01	Al_2O_3	11.19	8.80	11.93	12.25	10.96
Al_2O_3	20.82	21.41	21.57	21.21	21.36	Cr_2O_3	0.03	0.01	0.01	n.d.	n.d.
Cr_2O_3	0.02	n.d.	0.01	0.01	0.02	FeO	4.73	6.65	7.80	4.37	5.25
Y_2O_3	n.d.	0.03	n.d.	n.d.	n.d.	MnO	0.02	0.04	0.03	0.00	0.02
FeO	25.78	27.26	25.02	29.12	27.02	MgO	8.06	8.36	4.42	6.92	6.93
MnO	4.17	0.40	1.86	0.11	0.83	CaO	13.54	13.39	8.41	11.55	11.57
MgO	1.60	3.13	3.15	2.13	2.60	Na_2O	7.03	6.89	9.69	8.11	8.19
CaO	9.65	9.82	10.52	9.60	10.42	K_2O	n.d.	n.d.	n.d.	n.d.	n.d.
Total	99.55	100.27	100.49	100.06	100.37	Total	100.66	99.67	99.22	100.45	99.52
Si	2.992	3.000	2.998	2.999	2.995	Si	1.977	1.987	2.032	2.010	2.011
Al	1.966	1.983	1.990	1.985	1.982	AlIV	0.023	0.013	0.000	0.000	0.000
Ti	0.011	0.004	0.001	0.006	0.003	AlVI	0.442	0.358	0.502	0.508	0.459
Fe_{2+}	1.728	1.792	1.637	1.934	1.779	Ti	0.001	0.001	0.002	0.003	0.001
Cr	0.001	n.d	0.000	0.001	0.001	Cr	0.001	0.000	0.000	n.d.	n.d.
Mn	0.283	0.026	0.124	0.007	0.055	Fe_{3+}	0.060	0.130	0.099	0.019	0.081
Mg	0.191	0.367	0.368	0.253	0.305	Fe_{2+}	0.080	0.069	0.134	0.109	0.075
Ca	0.829	0.827	0.882	0.816	0.879	Mn	0.001	0.001	0.001	0.000	0.001
Y	n.d.	0.001	n.d.	n.d.	n.d.	Mg	0.424	0.447	0.235	0.363	0.367
Zr	n.d.	n.d.	0.000	0.000	0.000	Ca	0.512	0.514	0.322	0.435	0.441
O (calc)	11.986	11.996	11.994	11.997	11.990	Na	0.481	0.479	0.671	0.553	0.564
						K	n.d.	n.d.	n.d.	n.d.	n.d.
Alm	57.0	59.5	54.4	64.2	58.9	Jd	42.1	34.8	56.0	53.3	48.0
Pyp	6.3	12.2	12.2	8.4	10.1	CaTs	0.3	0.3	0.0	0.0	0.0
Grs	27.4	27.5	29.3	27.1	29.1	CaEs	0.0	0.0	0.0	0.0	0.0
Sps	9.3	0.9	4.1	0.2	1.8	Ess	0.3	0.4	0.0	0.0	0.0
$Mg/(Mg + Fe^{2+})$	9.9	17.0	18.3	11.6	14.7	Ac	5.7	12.8	11.1	2.0	8.4
						Di	43.0	44.5	20.5	33.5	36.6
						Hd	8.1	6.9	11.7	10.0	7.5

Garnet formulae normalized to 8 cations, all Fe = Fe^{2+}, Clinopyroxene formulae normalized to 8 cations and 6 oxygen to estimate Fe^{3+}

n.d. not detected

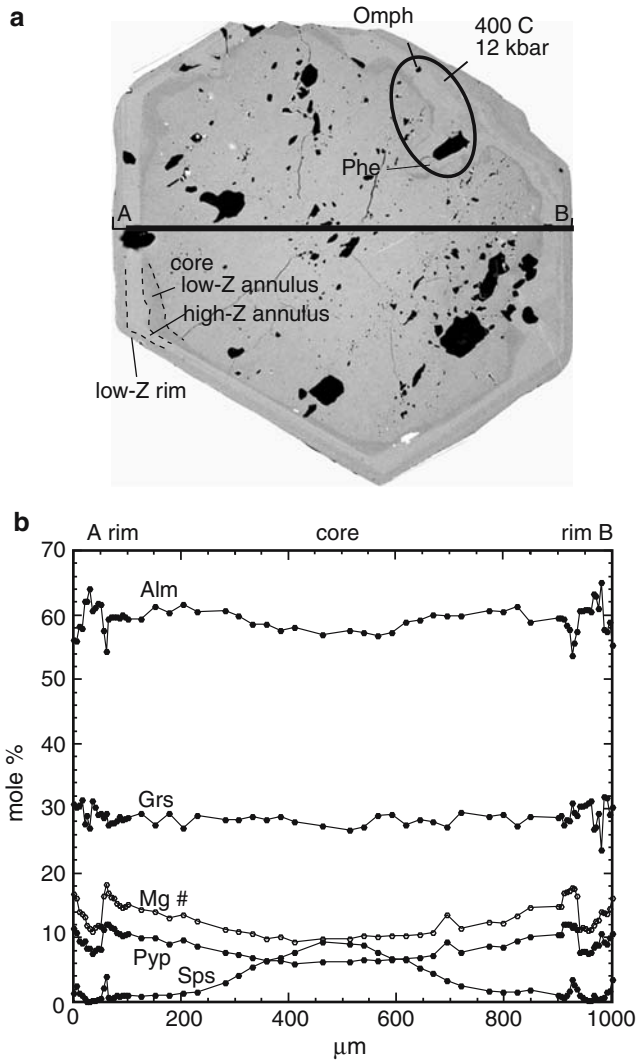

Fig. 5 Quantitative microprobe traverse of a garnet from a more retrogressed sample. Zoning in the core region is similar to that in less overprinted garnets (Fig. 4). The rim of this garnet found outside of the resorption boundary is characterized by sudden changes in chemistry. A high Mn, Mg, Ca, low Fe annulus partly fills in the resorbed garnet. Another high Fe, low Mn, Mg, Ca annulus fills in the rest of the corroded garnet. The outer, largely euhedral rim of the garnet is similar in composition to the high Mn annulus, but its margin with the high Fe annulus is less abrupt

annulus, a final low-Z stage is visible. This outermost rim is characterized by a more gradual decrease in Fe and rise in Ca, and with the reappearance of some Mn ($Alm_{59}Grs_{29}Pyp_{10}Sps_2$). The pyrope content slowly increases from high-Z annulus to the edge of the garnet (Fig. 5b). Fine-scale compositional variation within the zones demarcated above is visible in BSE (Fig. 5a). A similar zoning in garnet rims in eclogite hosted by the Franciscan from the Tiburon Peninsula was reported in the early microprobe study of garnet zoning by Dudley (1969) and more recently was described optically by Tsujimori et al. (2006).

Clinopyroxene

Zoning in matrix clinopyroxene is visible in BSE images (Figs. 2a, 3b, e, f, 6a) with distinctly high-Z rims on variably zoned low-Z cores. All clinopyroxenes are omphacite in composition, but show variation in Fe content that correlates with the BSE contrast (Fig. 6a, Table 1). Matrix omphacite contains inclusions of sphene and epidote. Small pits commonly found in the cloudy cores of matrix omphacite do not appear to be mineral inclusions in BSE imaging, and may be the remnants of fluid inclusions. Oriented quartz needles (often proposed as evidence of ultrahigh-pressure conditions; e.g., Liou et al. 1998) are not found in omphacite of the Junction School eclogite and have not been reported from any Franciscan occurrence. Omphacites are poor in the Ca-Tschermak's molecule and likely contain little to no Ca-Eskola component. A maximum of 10 mol% Ca-Eskola pyroxene is predicted for the unlikely case that all Fe is Fe^{3+}, but more reasonable estimates of Fe^{3+}, such as by calculation from stochiometry, yield no Ca-Eskola but significant acmite (Table 1). A microprobe traverse and BSE image (Fig. 6a) show a relatively sharp change from a typical core composition of $Di_{43}Jd_{42}Hd_8Ac_7$ to a typical rim

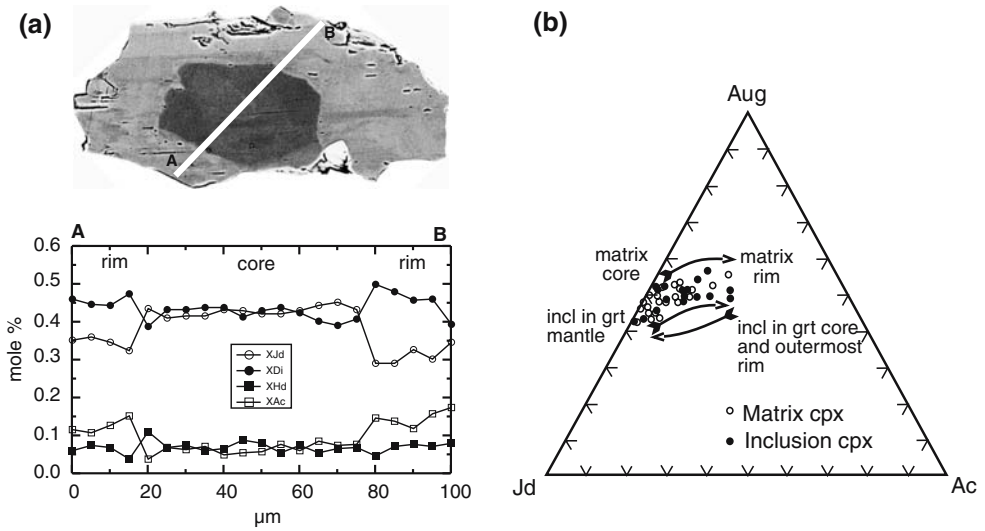

Fig. 6 Omphacite compositions. **a** BSE image and microprobe traverse of a matrix omphacite. Jadeite contents decrease and diopside and acmite contents increase abruptly from core to rim. **b** Omphacite compositions plotted on a ternary diagram. The cores of matrix omphacites contain less acmite and more jadeite than do the rims. The composition of clinopyroxene inclusions in garnet varies with position within the garnet. Inclusions in garnet cores and outermost rims have similar compositions to the rims of matrix omphacite. Inclusions in the mantles of garnet have a similar composition to the cores of matrix clinopyroxenes

composition of $Di_{45}Jd_{35}Hd_6Ac_{14}$. The Na content varies little from core to rim, and the shift from jadeite to acmite reflects replacement of Al by Fe^{3+}. Some omphacite rims show a slight decrease in diopside content with a concurrent increase in jadeite and acmite components from mantle to outermost rim. Individual clinopyroxene inclusions in garnet do not have internal zoning, and overall are slightly more sodic than matrix compositions. As with matrix clinopyroxene, variability in estimated Fe^{3+} content is greater than Na variability. Inclusions in the outermost annuli and rims of highly zoned garnets have compositions similar to nearby matrix omphacite rims (Table 1, Fig. 6b). Inclusion omphacite has apparently higher silica content than matrix compositions (Table 1), although this may be an artifact of secondary fluorescence. If the excess Si is an analytical artifact or evidence of a Ca-Eskola component, then Fe^{3+} will be underestimated and garnet-clinopyroxene temperatures will be overestimated.

Phengite

Phengitic muscovite is found both as a matrix phase and as an inclusion in the cores, mantles and outermost rims of garnet. In phengite, Mg and Fe^{2+} replace di-octahedral Al in a coupled substitution as Si replaces Al in the tetrahedral site to maintain charge balance. Limited solid solution exists between muscovite (Mu, $KAl_2AlSi_3O_{10}(OH)_2$) and mica end-members named for the clay mineral equivalents celadonite (Cel, $KAlMgSi_4O_{10}(OH)_2$) and ferroceladonite (Fcel, $KAlFe^{2+}Si_4O_{10}(OH)_2$, Li et al. 1997). Most workers do not estimate the Fe^{3+} content of these micas by stoichiometry because of uncertainties introduced by the possibility of variable VI or VIII vacancies and even O substitution for OH, and the commonly encountered and also ignored problems of beam damage in many of the published analyses would lead to spurious estimates. However, total Fe + Mg is greater than the excess tetrahedral Si (Fe + Mg > Si–3) in phengite from the Junction School eclogite (and many others, e.g., Sorensen et al. 1997; Nowlan et al. 2000; Wain et al. 2001; Ravna and Terry 2004), strongly suggesting the presence of Fe^{3+} as a ferrimuscovite (Fmu, $KFe^{3+}_2AlSi_3O_{10}(OH)_2$) component (Ahn et al. 1985, Giorgetti et al. 2000).

Paragonite has not been found in the rocks of this study. It is extremely rare in Franciscan eclogite and blueschist blocks (Essene 1967). Ahn et al. (1985) undertook a TEM and electron microprobe study of a single paragonite–phengite eclogite from Cazedero, California. This was the sole sample with paragonite identified by XRD from over a 100 blueschist and eclogite samples from the Franciscan by Essene (1967). Ahn et al. (1985) found that each mica grain has few if any intergrowths of the other at an ultrastructural level. In contrast, electron microprobe analyses of paragonite from Franciscan regional blueschist rocks (Pickett Peak Terrane) are dominated by submicroscopic intergrowths with phengite (Shau et al. 1991).

Phengite with variable Ba and K was reported in the Junction School eclogite and other Franciscan locali-

Table 2 Representative analyses of phengite, sphene, epidote and albite

	Phengite Matrix core	Phengite Matrix rim		Sphene Matrix	Sphene Rounded incl in grt	Sphene Euhedral in qz in grt		Epidote Inclusion in grt	Epidote Matrix	Epidote High-Z matrix	Albite Late vein
SiO_2	50.48	49.86	SiO2	31.22	30.40	30.86	SiO_2	38.59	38.11	37.15	67.08
TiO_2	0.11	0.15	TiO2	38.59	34.35	33.28	TiO_2	n.a.	n.a.	0.09	n.a.
V_2O_5	0.00	0.03	V_2O_5	n.a.	n.a.	n.a.	Al_2O_3	28.37	25.81	24.45	19.88
Al_2O_3	25.76	25.68	Al_2O_3	0.71	1.43	4.17	Cr_2O_3	n.a.	n.a.	n.a.	n.a.
Cr_2O_3	0.04	0.03	Cr_2O_3	n.a.	n.a.	n.a.	Fe_2O_3	7.54	10.45	9.45	0.73
FeO	3.28	4.17	Fe_2O_3	0.29	1.76	0.98	Ce_2O_3	0.02	0.06	1.00	n.a.
MnO	0.02	0.03	Ce_2O_3	0.03	n.d.	n.d.	Nd_2O_3	n.a.	n.a.	0.59	n.a.
MgO	3.66	3.38	Nd_2O_3	n.d.	n.d.	n.d.	Sm_2O_3	n.a.	n.a.	0.17	n.a.
CaO	0.03	0.00	FeO	n.a.	n.a.	n.a.	MnO	0.32	0.14	0.02	n.a.
BaO	0.64	1.33	MnO	n.a.	0.08	n.a.	MgO	n.a.	n.a.	0.20	n.a.
Na_2O	0.40	0.26	MgO	n.a.	0.05	n.a.	CaO	23.70	23.09	21.00	0.27
K_2O	11.03	10.62	CaO	28.08	30.77	28.74	SrO	n.d.	0.43	0.52	0.00
Cl	n.d.	n.d.	BaO	n.d.	n.d.	n.d.	BaO	n.d.	n.d.	0.04	0.06
F	n.d.	n.d.	Na_2O	n.d.	n.d.	n.d.	Na_2O	n.a.	n.a.	n.a.	11.82
H_2O calc	5.30	5.35	K_2O	n.d.	n.d.	n.d.	K_2O	n.a.	n.a.	n.a.	0.02
			Cl	n.a.	n.a.	n.a.					
			F	0.02	0.11	1.36					
			H_2O calc	0.29	0.79	0.40					
Total	100.74	100.87	Total	99.23	99.72	99.26	Total	98.44	98.09	94.68	99.86
Si	6.795	6.738	Si	1.000	1.000	1.000	Si	2.986	2.998	3.054	2.950
Al_{IV}	1.205	1.262	AlIV	n.c.	n.c.	n.c.	Al	2.587	2.393	2.369	1.030
Al_{VI}	2.880	2.828	AlVI	0.027	0.055	0.159	Fe_{3+}	0.439	0.619	0.585	0.024
Fe total	0.369	0.471	Fe total	0.007	0.043	0.024	Mn	0.019	0.009	0.001	n.c.
Mn	0.002	0.003	Mn	0.000	0.002	0.000	Mg	n.c.	n.c.	0.016	n.c.
Mg	0.734	0.680	Mg	0.000	0.002	0.000	Ca	1.965	1.947	1.850	0.013
Ti	0.011	0.015	Ti	0.930	0.850	0.811	Sr	n.c.	0.023	0.029	0.000
Cr	0.004	0.003	Cr	n.c.	n.c.	n.c.	Ba	0.000	0.000	0.001	0.001
Ca	0.004	0.000	Ca	0.964	1.084	0.998	Na	n.c.	n.c.	n.c.	1.008
Na	0.104	0.067	Na	0.000	0.001	0.000	K	n.c.	n.c.	n.c.	0.001
K	1.894	1.830	K	0.000	0.001	0.000	Ce	0.001	0.002	0.030	n.c.
Ba	0.034	0.071	Ba	0.000	0.000	0.000	Nd	n.c.	n.c.	0.017	n.c.
			O calc	4.873	4.932	4.825	Sm	n.c.	n.c.	0.005	n.c.
			F	0.002	0.011	0.139	Cz	85.6	79.5	79.7	n.c.
			OH	0.032	0.087	0.044	Ps	14.4	20.5	19.7	n.c.
			Sum cations	2.927	3.039	2.992	Ab	n.c.	n.c.	n.c.	98.6
							An	n.c.	n.c.	n.c.	1.2
							Or	n.c.	n.c.	n.c.	0.0

Phengite formulae normalized to 12 ''small'' cations (not including K, Na, Ca, Ba, Sr), Sphene formulae normalized to 1 Si, OH=5-O–F, Epidote normalized to 8.5 oxygen, Albite formula normalized to 8 oxygen

n.a. not analyzed, *n.d.* not detected, *n.c.* not calculated

ties by Sorenson et al. (1997). Matrix phengite in the Junction School eclogite, is zoned in both ferroceladonite (Fcel) and ferrimuscovite (Fmu) (Table 2, Fig. 7a) as well as in minor Na (paragonite, Pa, $NaAl_2AlSi_3O_{10}(OH)_2$), and Ba (ganterite, Gan, $BaAl_2Al_2Si_2O_{10}(OH)_2$, Graeser et al. 2003). Phengite cores ($Mu_{39}Fmu_{11}Cel_{37}Fcel_7Pa_5Gan_2$) have higher concentrations of Cel, Fcel and Pa, whereas the mantles ($Mu_{36}Fmu_{18}Cel_{34}Fcel_5Pa_3Gan_4$) and rims are enriched in Gan and Fmu. Both Pa and Gan decrease from the core to mantle regions of the phengite, and both abruptly increase (Ba > Na) in the mantle region. Gan and Pa components then decrease from the mantle peak to the rim (Fig. 7b). The systematic nature of the zoning in matrix phengite is not in support of the assertion by Sorenson et al. (1997) that Ba and Na do not vary systematically from core to rim in matrix phengite in the Franciscan. Phengite inclusions ($Mu_{32}Fmu_{15}Cel_{36}Fcel_{15}Pa_1\ Gan_0$) in garnet are distinguished from matrix compositions by lower Gan and Pa contents (Fig. 7b).

Sphene

Matrix sphene is compositionally distinct from sphene inclusions in garnet (Table 2, Fig. 8). Matrix sphene has patchy compositional zoning in Al and less Fe than the inclusions in garnet. Most sphene inclusions are

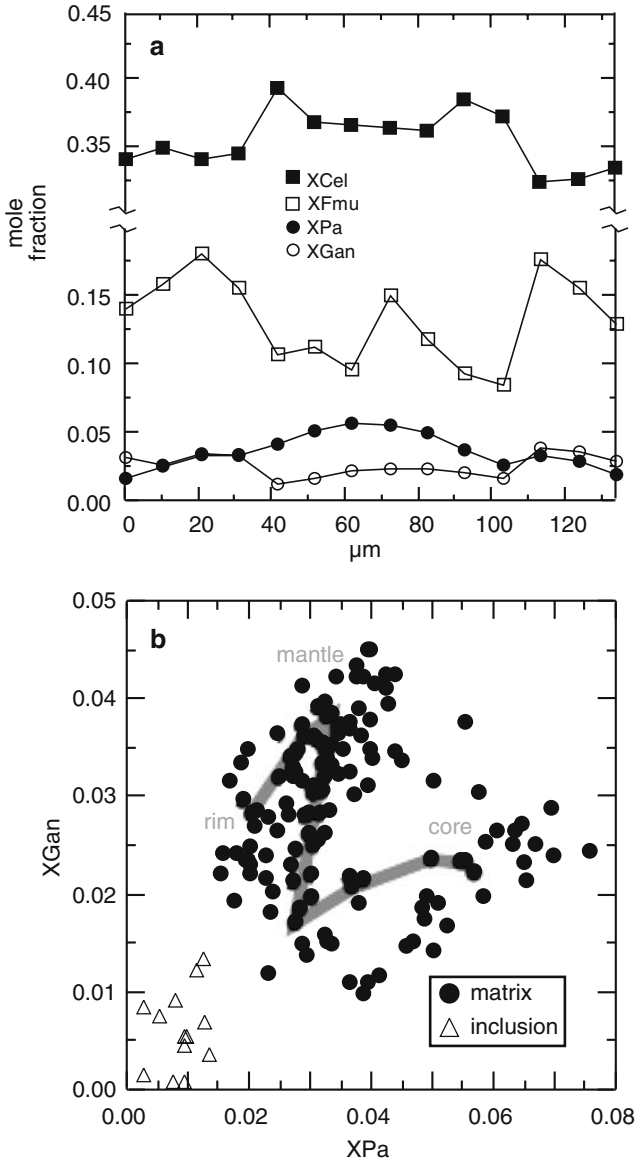

Fig. 7 Phengite compositions. **a** Microprobe traverse of a matrix phengite. Phengites have nearly constant ferroceladonite and muscovite components (omitted for clarity). Within the cores of phengite, celadonite slightly increases as ferrimuscovite, paragonite and ganterite decrease. In the mantles, ferrimuscovite, ganterite, and paragonite suddenly increase as celadonite falls. Ganterite invariably increases more than paragonite at this discontinuity, and often surpasses paragonite in concentration. The zoning pattern of the core then repeats itself as celadonite increases or remains steady and ferrimuscovite, ganterite and paragonite decrease from mantle to rim. **b** Phengite inclusions in garnet are chemically distinct from matrix phengites because of their low paragonite and ganterite contents. Tie lines illustrate the zoning of the phengite traverse shown in (**a**)

rounded (Fig. 2c), and as a population, have a slightly larger variation in Al than the matrix. Armstrong et al. (2004) reported a similar variation in sphene from a nearby, more heavily overprinted eclogite block, but also found a second population of sphene inclusions with significantly higher Al and OH. No such high-Al sphenes were found in the block in this study. However, in two garnets, euhedral sphene was observed in quartz inclusions in garnet (Fig. 2d). These sphene grains have a composition with higher Al and F than other examples of the mineral in this rock.

Other minerals

Epidote occurs as a late matrix phase and as inclusions in garnet (Table 2). Matrix epidotes have an average composition of $Cz_{79}Ps_{21}$ and many have patchy zoning in Sr and the rare earth elements (REE). Epidote inclusions in garnet have less Fe^{3+} ($Cz_{85}Ps_{15}$) with little compositional variation and negligible Sr and REE in garnet cores. In garnet rims, epidote has some patchy zoning in Sr, and similar Ps contents to epidote inclusions in garnet cores. Plagioclase occurs as late veins rimming or cutting through garnet (Fig. 3e). In all cases, the feldspar is almost pure albite in composition (Table 2). Unlike the inferences of Wakabayashi (1990), the authors of this paper do not think that albite was part of the eclogite stage assemblage in the samples under study.

Thermobarometry

Prograde

A fragmented record of the prograde mineralogy of an eclogite is sometimes preserved in the inclusions entrapped in garnet during its growth. These minerals (and their host garnet) are sequestered from the majority of the rock that continues to recrystallize. Chemical zonation in garnet allows inclusions from various stages of the early history of the eclogite to be grouped together as metamorphic assemblages and their conditions of formation calculated. Inclusion assemblages chosen for thermobarometry occur close to one another in garnets or within contiguous zones of similar chemistry. After entrapment, the possibility exists for included phases and the host garnet to re-equilibrate under changing *P–T* conditions. Resorption of the garnet indicates reaction of earlier garnet with the matrix and/or an introduced fluid, and it cannot be included in thermobarometry for or following that event. Net transfer reactions are often accompanied by a volume change, and therefore inclusions are monitored for radial fractures in the garnet. Because an increased number of minerals in contact with one another increases the likelihood of reaction, simple inclusions

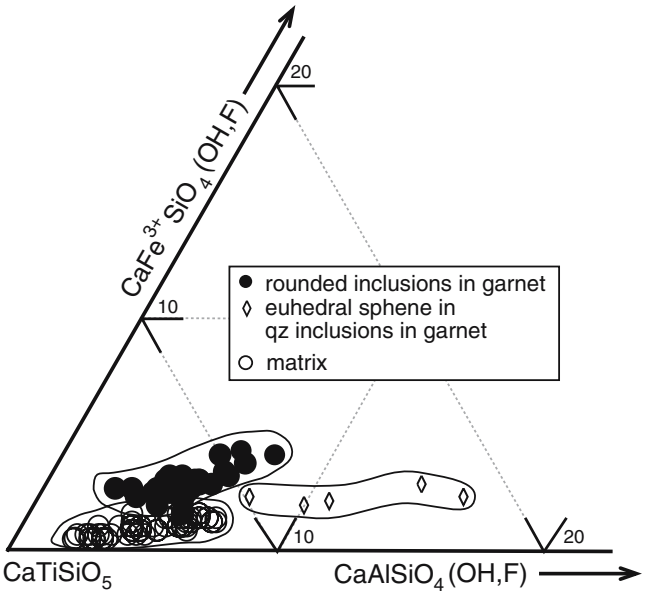

Fig. 8 Sphene compositions. Matrix sphene and inclusions in garnet have slightly overlapping compositional fields, but in general sphene inclusions contain more Al and Fe^{3+}. Euhedral sphene inclusions in quartz inclusions in garnet (Fig. 2d) contain notably more Al and F

are preferred to compound inclusions. A lack of fracturing around many inclusions coupled with minimal zoning in the garnet surrounding them is taken as evidence that no net transfer reaction has taken place. This cannot be said for exchange reactions, which may have reequilibrated along the retrograde path, leaving no textural evidence other than chemical halos around the inclusion (Wang et al. 1999).

The cores of garnet in the Junction School eclogite often contain the assemblage epidote–sphene–rutile–quartz, which allows application of the reaction:

$$\begin{aligned}\text{clinozoisite} + \text{sphene} &= \text{grossular} + \text{rutile} \\ &\quad + \text{quartz} + H_2O\end{aligned} \qquad (1)$$

$$2Ca_2Al_3Si_3O_{12}(OH) + 5CaTiSiO_5 = 3Ca_3Al_2Si_3O_{12} + 5TiO_2 + 2SiO_2 + H_2O$$

a variation on the zoisite reaction proposed as a barometer by Manning and Bohlen (1991). This dehydration reaction has a flat slope in P–T space at lower temperatures (Manon et al. 2006). It acts as a barometer with a slightly negative slope in the temperature range of interest in this study for the measured compositions of epidote, sphene, grossular and rutile. At higher T/P, the metastable extension of this reaction (outside the stability field of clinozoisite) steepens, becomes vertical, then assumes a shallow positive slope, returning to the origin at very low P. As equilibrium (1) is a dehydration reaction, its locus shifts with aH_2O However, hydrous inclusions (mica, epidote) are found throughout garnet with minimal halogen contents and a high water activity is expected in a subduction-zone environment. Reduction of aH_2O to 0.8 has the effect of reducing pressures by approximately 1 kbar. The activity of $CaTiSiO_5$ in sphene was calculated using a simple molecular model ($a_{CaTiSiO_5} = X_{Ti}$) as suggested by Tropper et al. (2002) for low-Al sphene. The ideal coupled ionic model ($a_{CaTiSiO_5} = X_{Ca}X_{Ti}X_{Si}X_{O1}$) more recently proposed by Tropper et al. (2006) for low temperature equilibria reduces $a_{CaTiSiO5}$ for those sphenes used in thermobarometry by 0.01–0.05, resulting in pressure increases of <1 kbar. The activity of TiO_2 in rutile was also calculated assuming ideal molecular mixing (Essene 1989). The activity of $Ca_2Al_3Si_3O_{12}(OH)$ in epidote was calculated using the a/X program of Holland and Powell (1998). The $Ca_3Al_2Si_3O_{12}$ activity in garnet was calculated using the quaternary mixing model of Ganguly et al. (1996). The locus of reaction (1) was calculated using the updated Holland and Powell (1998) thermodynamic database adjusted to reflect new estimates of the heat capacity of sphene (Manon and Essene 2005; Manon et al. 2006). The locus of equilibrium (1) calculated with the Holland and Powell (1998) database underestimates P by 1–2 kbar without new thermodynamic data for sphene. This barometer provides a range of pressures (7–22 kbar) from instances of this assemblage in garnet cores and mantles (Fig. 9a). Higher pressures from the mantle region of the garnet result primarily from increasing dilution of $CaTiSiO_5$ in sphene by $Ca(Al,Fe^{3+})SiO_4OH$ from $a_{CaTiSiO_5} = 0.96$ in garnet cores to $a_{CaTiSiO_5} = 0.84$ in garnet rims. In principle, the K_D of an exchange reaction of Fe^{3+} and Al between epidote, garnet and/or sphene could serve as a thermometer in this assemblage, which would lead to a unique solution of both P and T, but no such thermometer has yet been

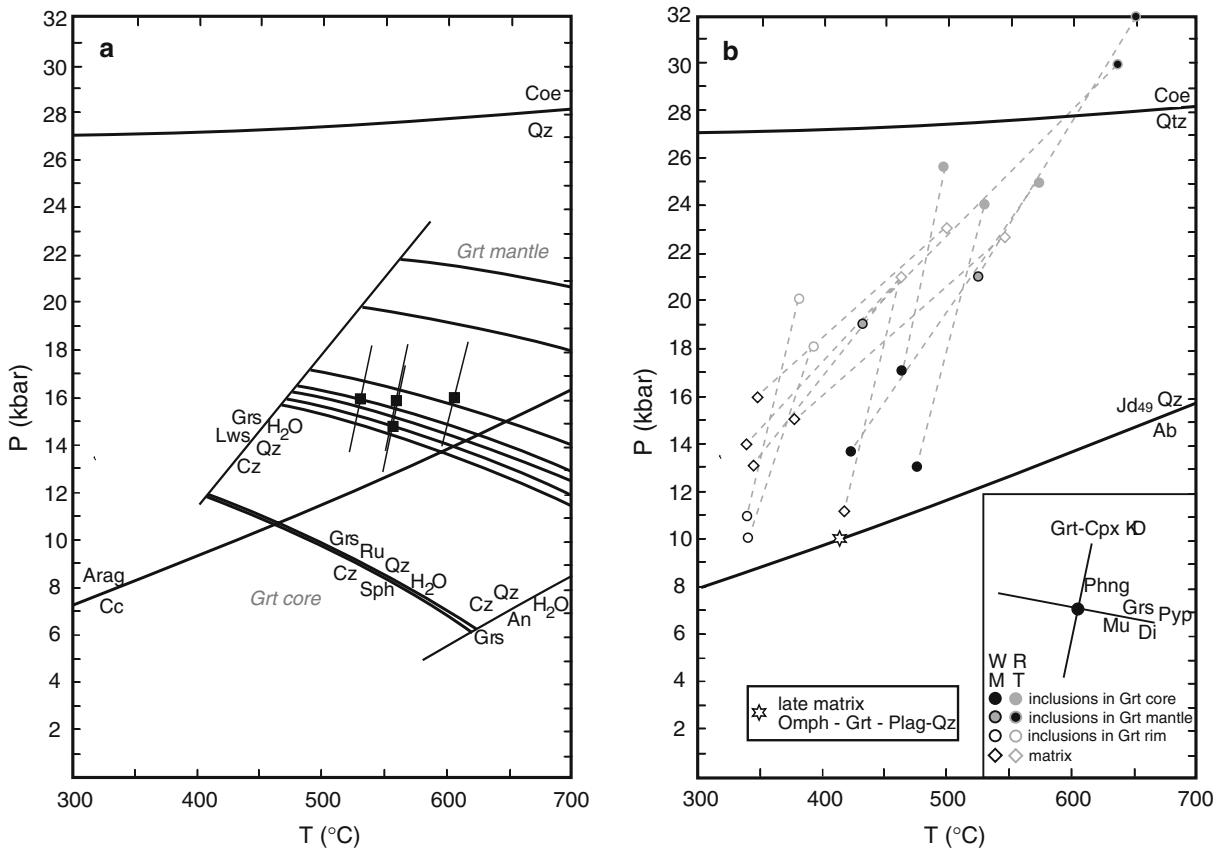

Fig. 9 Thermobarometry. **a** The loci for equilibrium (1) corrected for solid solutions of the constituent phases are plotted within the stability field of epidote. When omphacite is part of the inclusion assemblage, the intersection of the garnet–clinopyroxene thermometer (Ravna 2000) and the curves for equilibrium (1) are marked with *solid squares*. Equilibria (2) and (3) provide temperature limits when omphacite is not part of the inclusion assemblage. **b** Garnet–phengite–clinopyroxene thermobarometry. Points in *P–T* space represent the intersection of garnet–clinopyroxene K_D thermometry (Ravna 2000) and garnet–phengite–clinopyroxene barometry using two different calibrations: Waters and Martin (WM *darker symbols*) and Ravna and Terry (RT *lighter symbols*). *P–T* estimates from the same mineral compositions are joined by light gray tie lines. The textural location of the reaction assemblage and representative geometry of the intersection are found in the inset. The six-pointed star represents the intersection of garnet–clinopyroxene thermometry and the fully buffered albite–clinopyroxene–quartz barometer for the late matrix assemblage

calibrated. In the absence of another phase suitable for thermometry (e.g., omphacite or phengite), temperature limits for the assemblage of equilibrium (1) can be made from the stability of clinozoisite–quartz±fluid (Newton 1966; Perkins et al. 1980).

$$\text{grossular} + \text{lawsonite} = \text{clinozoisite} + \text{quartz} + H_2O \quad (2)$$

$$Ca_3Al_2Si_3O_{12} + 5CaAl_2Si_2O_7(OH)_2.H_2O = 4Ca_2Al_3Si_3O_{12}(OH) + SiO_2 + 8H_2O$$

$$\text{clinozoisite} + \text{quartz} = \text{grossular} + \text{anorthite} + H_2O \quad (3)$$

$$4Ca_2Al_3Si_3O_{12}(OH) + SiO_2 = Ca_3Al_2Si_3O_{12} + 5CaAl_2Si_2O_8 + 2H_2O$$

The loci of reactions (2) and (3) were calculated using THERMOCALC with unit activities for lawsonite, anorthite and H_2O, which constrains the temperature range of these inclusions to between 375 and 600°C at low *P* (Fig. 9a). At higher *P*, equilibrium (3) no longer provides a useful constraint on *T* because the locus of the reaction shifts to unreasonably high *T* for these rocks (700–900°C). The presence of omphacite inclusions near the reaction assemblage of equilibrium (1) in the mantle regions of garnet allows the application of exchange thermometry (Fe^{2+}/Mg) between inclusions of omphacite and the host garnet. Omphacite–garnet pairs yield temperatures of 525–600°C using the thermometer of Ravna (2000), at 14–15 kbar given by equilibrium (1). Retrogressive resetting of exchange thermometers is possible due to diffusional exchange of Fe^{2+}/Mg. These omphacite inclusions are not zoned,

although unzoned olivine inclusions in garnet have been documented to exchange Fe^{2+}/Mg with their host, leaving a halo of Fe^{2+}/Mg zoning in the surrounding garnet (Wang et al. 1999). Detailed microprobe traverses around these inclusions fail to reveal any such halos, and it is assumed that these are restricted to narrow submicroscopic zones on the edges of the inclusions, or that diffusion was minimal. The absence of chemical halos around omphacite inclusions and retention of a detailed zoning pattern across garnet suggests $T < 700$°C for these rocks that likely inhibits resetting of thermometers.

Phengite inclusions are also occasionally found in garnets from the Junction School eclogite. A relatively recent development in the thermobarometry of eclogites is the calibration of the garnet–phengite–clinopyroxene thermobarometer (Waters and Martin 1993) that makes use of the celadonite component in phengitic muscovite in equilibrium with pyroxene and garnet:

$$\text{diopside} + \text{muscovite} = \text{grossular} + \text{pyrope} + \text{celadonite} \quad (4)$$

$$\begin{aligned} &6CaMgSi_2O_6 + 3KAl_2AlSi_3O_{10}(OH)_2 \\ &\quad = 2Ca_3Al_2Si_3O_{12} + Mg_3Al_2Si_3O_{12} \\ &\quad + 3KMgAlSi_4O_{10}(OH)_2 \end{aligned}$$

This reaction has a slightly negative slope in P–T space for typical compositions, and, when coupled with garnet–clinopyroxene thermometry from the same assemblage puts constraints on both P and T. Garnet–omphacite–phengite inclusion sets were found in the core, mantle, and rim regions of garnets, and their P–T of formation were calculated with the Ravna (2000) thermometer, the updated semi-empirical calibration of the Waters–Martin barometer (Wain et al. 2001) and the fully thermodynamic calibration of Ravna and Terry (2004). The Waters–Martin (WM) calibration is based on the Holland and Powell (1990) data set with an empirical correction relative to observed coesite versus quartz in natural samples. It uses ideal molecular mixing for phengite, and estimated Fe^{3+} in both pyroxene and mica, the Holland (1990) model for clinopyroxene, and a simple Ca–Mg mixing model for garnet (Newton and Haselton 1981). Although the thermodynamic data set and garnet mixing models used in this calibration are out of date, they were employed for the sake of consistency with the empirical correction inherent to this model. Garnet, clinopyroxene and phengite compositions used in thermobarometry are reported in Table 3. Using the WM barometer, phengite inclusions in the cores of garnets yield pressures of 13–17 kbar over a temperature range of 400–500°C (Fig. 9b), similar results to the sphene–rutile barometer (equilibrium 1) for inclusions in garnet cores (Fig. 9a). Phengite barometry on inclusions in the mantle regions of garnet yields pressures of 19–21 kbar over 450–550°C, similar to the P calculated by equilibrium (1) for inclusions in garnet mantles (Fig. 9a, b).

The most recent calibration of this barometer (Ravna and Terry 2004, RT) is based exclusively on an updated version of the Holland and Powell (1998) database. Calculations of the locus of equilibrium (4) using the RT calibration yield pressures of 24–32 kbar from 500–650°C (Fig. 9b). Clearly there is a major discrepancy between these two calibrations of the garnet–phengite–clinopyroxene barometer at least for the mineral compositions found in these rocks.

Peak conditions

In many studies of eclogite, a lower bound for peak pressures is given by:

$$\begin{aligned} \text{albite} &= \text{jadeite} + \text{quartz} \\ NaAlSi_3O_8 &= NaAlSi_2O_6 + SiO_2 \end{aligned} \quad (5)$$

in the absence of plagioclase. However, quartz does not appear to be in equilibrium with matrix omphacite in the Junction School block. Quartz in the Junction School eclogite appears only as inclusions in garnet and as texturally late veins and in interstitial spaces between euhedral grains of matrix omphacite and garnet. Even if quartz is assumed to be present, the matrix omphacite with the highest jadeite content (Jd_{56}) yields a minimum P of 15 kbar at 600°C (garnet mantle–pyroxene core K_D thermometry), well below pressures recorded by inclusions in the garnet mantles. Thus, equilibrium (5) provides constraints of only limited value on the peak pressures of metamorphism. Matrix phengite appears texturally late in the history of the Junction School eclogite, likely in equilibrium with clinopyroxene and garnet rims but not with the peak assemblage. The classic high-variance eclogite assemblage continues to paralyze attempts to constrain the peak P–T of the Junction School eclogite.

Retrograde

The Junction School eclogite does not contain the pervasive glaucophane retrogression of many other eclogites hosted by the Franciscan formation (e.g., Krogh et al. 1994). However, retrogression certainly did take place, and is recorded both in the rims of some

garnets, and in the texturally late assemblage of omphacite rim, phengite rim and garnet rim with the matrix assemblage epidote + chlorite + sphene + zircon ± albite ± calcite/aragonite ± glaucophane. Phengite and omphacite rims appear to be in equilibrium with some garnet rims, and yield retrograde *P–T* of 11–16 kbar over 350–400°C via equilibrium (4) and the WM calibration. The RT calibration yields conditions of 21–23 kbar at 450–500°C. Omphacite and phengite inclusions in the rims of garnet yield similar conditions, reinforcing textural evidence of continued garnet growth during retrogression after a period of garnet resorption (Fig. 9b).

Albite, omphacite and quartz veins growing in apparent equilibrium with euhedral late garnet rims (Fig. 3e) fully buffer the classic eclogite barometer (equilibrium 5) as well as the garnet–clinopyroxene exchange thermometer. They yield conditions of 10 kbar and 400°C with plagioclase of composition Ab_{99} and omphacite with Jd_{47} (Fig. 9b).

Table 3 Garnet, clinopyroxene and phengite analyses used for thermobarometry

	Matrix	Matrix	Matrix	Matrix	Matrix	Incl Core	Incl Core	Incl Core	Incl Mantle	Incl Mantle	Incl Rim	Incl Rim
Garnet analyses[a]												
SiO_2	37.33	38.38	37.90	38.08	38.53	37.80	38.34	37.64	37.50	38.45	38.03	38.49
TiO_2	0.03	n/d	0.08	n/d	n/d	0.09	0.08	0.13	0.11	0.17	0.06	0.11
Al_2O_3	21.23	21.75	21.64	21.52	21.53	21.56	21.49	21.75	21.38	20.68	21.18	21.09
Cr_2O_3	0.02	0.00	-0.01	0.01	0.04	0.00	0.04	0.00	0.05	0.04	0.03	-0.01
FeO	26.09	27.65	26.40	28.08	27.61	25.48	26.55	26.20	25.65	24.91	27.21	26.55
MnO	1.05	0.45	0.29	0.71	0.74	3.71	1.55	1.76	0.42	1.04	0.19	0.44
MgO	3.61	3.08	3.37	2.90	3.42	2.03	2.43	2.15	2.69	3.25	2.01	2.29
CaO	9.45	8.14	9.97	9.53	8.94	8.88	9.45	10.41	10.83	11.09	10.75	10.04
Total	98.97	99.53	99.77	100.85	100.82	99.61	100.05	100.10	98.97	100.48	99.47	99.01
Si	2.97	3.05	2.99	2.98	3.01	3.02	3.04	2.98	2.99	3.03	3.03	3.07
Al	1.99	2.03	2.01	1.99	1.98	2.03	2.01	2.03	2.01	1.92	1.99	1.99
Ti	0.00	0.00	0.00	0.00	0.00	0.01	0.00	0.01	0.01	0.01	0.00	0.01
Fe_{2+}	1.74	1.83	1.74	1.84	1.80	1.70	1.76	1.73	1.71	1.64	1.81	1.77
Cr	0.00	0.00	0.00	0.00	0.00	0.00	0.00	0.00	0.00	0.00	0.00	0.00
Mn	0.07	0.03	0.02	0.05	0.05	0.25	0.10	0.12	0.03	0.07	0.01	0.03
Mg	0.43	0.36	0.40	0.34	0.40	0.24	0.29	0.25	0.32	0.38	0.24	0.27
Ca	0.81	0.69	0.84	0.80	0.75	0.76	0.80	0.88	0.93	0.94	0.92	0.86
O (calc)	11.97	12.06	12.00	11.98	12.01	12.03	12.05	12.00	12.01	12.01	12.03	12.07
Alm	57	63	58	61	60	58	60	58	57	54	61	60
Pyp	14	12	13	11	13	8	10	8	11	13	8	9
Grs	26	24	28	26	25	26	27	30	31	31	31	29
Sps	2	1	1	2	2	8	4	4	1	2	0	1
Clinopyroxene analyses[b]												
SiO_2	55.22	55.84	56.08	55.86	55.99	54.91	55.95	55.76	54.79	55.13	56.21	56.33
TiO_2	0.05	0.02	0.02	0.00	0.00	0.03	0.00	0.09	0.02	0.05	0.02	0.06
Al_2O_3	8.15	9.92	9.14	9.57	8.33	8.28	9.49	11.43	9.20	8.34	10.88	11.14
Cr_2O_3	0.03	0.00	0.07	0.01	-0.01	0.00	0.00	0.01	0.00	0.04	0.02	0.00
FeO	7.76	6.16	6.89	7.02	7.24	11.08	6.72	6.28	8.75	8.84	5.94	6.51
MnO	0.06	0.04	0.05	0.16	0.06	0.21	0.06	0.05	0.12	0.15	0.02	0.03
MgO	8.57	8.13	8.43	7.57	8.67	5.98	8.10	7.20	6.68	7.72	6.82	7.59
CaO	14.15	12.31	13.79	12.84	14.05	10.32	12.07	12.93	12.93	13.23	11.49	13.12
Na_2O	6.65	7.15	7.08	7.52	6.83	8.23	7.07	7.43	7.22	7.16	8.13	7.79
K_2O	0.01	0.01	0.00	0.00	0.00	0.05	0.00	0.01	0.00	0.00	0.01	0.02
Total	100.67	99.67	101.55	100.55	101.18	99.10	99.54	101.20	99.74	100.69	99.54	102.68
Si	1.97	2.00	1.97	1.98	1.98	1.99	2.01	1.96	1.98	1.97	2.00	1.95
Al	0.34	0.42	0.38	0.40	0.35	0.35	0.40	0.47	0.39	0.35	0.46	0.45
Fe_{3+}	0.18	0.09	0.16	0.15	0.16	0.24	0.08	0.10	0.16	0.21	0.10	0.16
Fe_{2+}	0.05	0.10	0.04	0.05	0.05	0.10	0.12	0.08	0.10	0.06	0.08	0.03
Mg	0.45	0.43	0.44	0.40	0.46	0.32	0.43	0.38	0.36	0.41	0.36	0.39
Ca	0.54	0.47	0.52	0.49	0.53	0.40	0.46	0.49	0.50	0.51	0.44	0.49
Na	0.46	0.50	0.48	0.52	0.47	0.58	0.49	0.51	0.50	0.50	0.56	0.52
Jd	29	41	33	37	31	35	41	41	35	30	46	37
Di	48	38	47	43	48	31	36	40	39	44	36	46
Hd	6	9	5	6	5	9	10	9	11	6	8	3
Ac	17	8	15	15	16	23	8	9	15	20	10	15

Table 3 Continued

	Matrix	Matrix	Matrix	Matrix	Matrix	Incl Core	Incl Core	Incl Core	Incl Mantle	Incl Mantle	Incl Rim	Incl Rim
Phengite analyses and *P–T* comparison[c]												
SiO_2	50.30	49.02	49.38	50.15	50.35	51.27	51.22	51.13	51.01	52.63	49.49	50.23
TiO_2	0.10	0.04	0.08	0.09	0.03	0.00	0.00	0.03	0.02	n.d.	0.18	0.15
Al_2O_3	25.52	26.03	24.91	25.39	25.67	23.46	21.97	23.36	21.44	21.76	28.26	25.68
Cr_2O_3	0.01	0.02	n.d.	0.00	n.d.	0.03	0.03	0.04	0.02	0.03	0.00	0.01
FeO	3.55	4.52	3.92	3.99	4.09	4.83	5.34	5.10	6.62	6.45	3.77	4.14
MnO	0.06	0.04	-0.03	0.06	0.05	0.12	0.11	0.09	0.10	0.05	0.00	0.01
MgO	3.40	3.18	3.55	3.48	3.39	3.47	3.47	3.28	3.51	2.97	3.11	3.28
CaO	0.02	0.00	0.07	0.00	n.d.	0.01	0.02	0.01	0.49	0.07	0.01	0.05
BaO	0.97	0.57	0.72	0.97	1.20	0.21	0.06	0.35	0.28	0.14	0.15	0.86
Na_2O	0.24	0.25	0.13	0.23	0.22	0.07	0.02	0.06	0.04	0.10	0.62	0.27
K_2O	10.85	10.54	10.26	10.85	11.31	11.03	11.02	10.72	10.20	10.60	11.05	11.42
Cl	0.01	0.01	0.01	0.01	n.d.	0.01	0.02	0.04	0.01	n.d.	0.01	0.02
F	0.08	0.03	0.13	0.00	n.d.	0.07	0.00	n.d.	0.01	n.d.	0.00	0.05
Total	95.13	94.27	93.16	95.22	96.31	94.57	93.27	94.22	93.75	94.85	96.70	96.20
IV												
Si	6.82	6.66	6.79	6.78	6.78	6.97	7.08	6.98	7.02	7.16	6.55	6.77
Al	1.18	1.34	1.21	1.22	1.22	1.03	0.92	1.02	0.98	0.84	1.45	1.23
VI												
Al	2.89	2.83	2.82	2.83	2.85	2.73	2.65	2.73	2.50	2.66	2.95	2.86
Fe_{3+}	0.22	0.51	0.45	0.33	0.25	0.34	0.31	0.36	0.49	0.28	0.42	0.20
Fe_{2+}	0.18	0.00	0.00	0.12	0.21	0.21	0.31	0.22	0.27	0.46	0.00	0.27
Mg	0.69	0.64	0.73	0.70	0.68	0.70	0.72	0.67	0.72	0.60	0.61	0.66
Ti	0.01	0.00	0.01	0.01	0.00	0.00	0.00	0.00	0.00	0.00	0.02	0.02
Mn	0.01	0.00	0.00	0.01	0.01	0.01	0.01	0.01	0.01	0.01	0.00	0.00
Cr	0.00	0.00	0.00	0.00	0.00	0.00	0.00	0.00	0.00	0.00	0.00	0.00
X												
K	1.88	1.83	1.80	1.87	1.94	1.91	1.94	1.87	1.79	1.84	1.87	1.96
Na	0.06	0.07	0.03	0.06	0.06	0.02	0.00	0.02	0.01	0.03	0.16	0.07
Ca	0.00	0.00	0.01	0.00	0.00	0.00	0.00	0.00	0.07	0.01	0.00	0.01
Ba	0.05	0.03	0.04	0.05	0.06	0.01	0.00	0.02	0.02	0.01	0.01	0.05
P: Waters and Martin (1996) (Wain et al. 2001); *T*: Ravna (2000)												
P (kbar)	15	11	16	13	14	13	17	15	21	19	10	11
T (°C)	378	412	353	343	340	477	465	426	528	437	340	340
P, *T*: Ravna and Terry (2004)												
P (kbar)	23	21	23	21	21	24	27	25	32	30	18	20
T (°C)	546	461	505	458	461	537	497	570	651	632	391	483

n.d. not detected

[a] Garnet formulae normalized to 8 cations, all Fe = Fe^{2+}

[b] Clinopyroxene formulae normalized to 8 cations and 6 oxygens to estimate Fe^{3+}

[c] Phengite formulae normalized to 12 ''small'' cations (not including K, Na, Ca, Ba, Sr) and 22 O

P–T path

Collectively, the data presented here constrain both a prograde and retrograde *P–T* path for the Junction School eclogite (Fig. 10). Two independent barometers (equilibria 1 and 4) used with inclusions in garnet give consistent results with 7–15 kbar garnet core assemblages (~450°C), followed by 18–22 kbar for the garnet mantle (550°C) if the empirically corrected WM calibration is used for garnet–clinopyroxene–phengite thermobarometry (Table 3, Fig. 10). If the fully thermodynamic RT calibration is used, phengite and clinopyroxene inclusions in garnet trace a somewhat shallower *P*/*T* prograde path at higher *P* and *T* (~25 kbar at 550°C in garnet cores to 30–32 kbar at 650°C in garnet mantles). Prograde pressures yielded by the RT barometer are 10–15 kbar higher than those recorded by equilibrium (1) by inclusions found at similar relative positions in garnet. The peak *P–T* of metamorphism is poorly constrained, but because of the rather complete record of pressures on the prograde path, it seems unlikely that a significantly higher pressure was attained without some evidence preserved. Certainly there is no evidence of former coesite based on lack of palisade textures or clear radial fractures. Raman spectrometry and electron backscattered

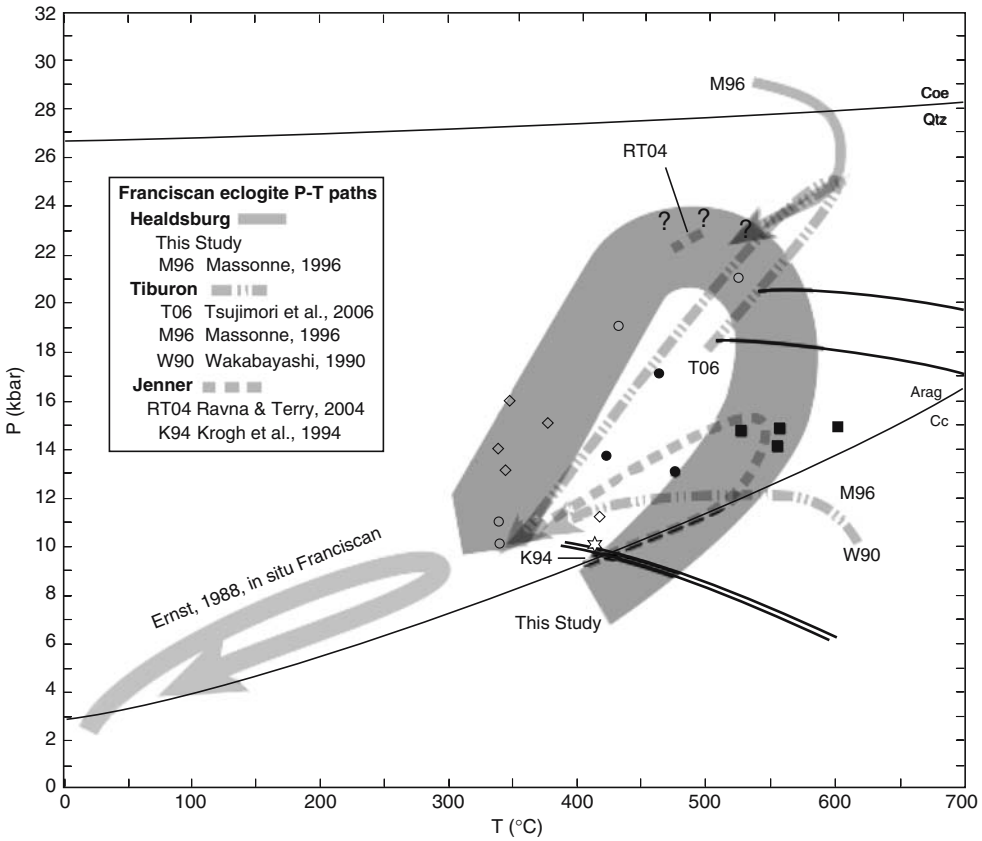

Fig. 10 *P–T* paths. Thermobarometric estimates are summarized from Fig. 9 using the same symbology. Pressure estimates from inclusion assemblages using both equilibria (1) and (5) with the Waters and Martin calibration yield similar results. Inclusions define a steep prograde path despite a ~150°C spread in temperatures. Inclusions in the rims of zoned garnets and late matrix phengite, omphacite and garnet rims constrain retrograde event(s) at 9–16 kbar, 350–400°C. No thermobarometric estimates were possible for the peak of metamorphism, but, because of the generally low *T*, a steep retrograde path would seem to be the only likely possibility. *P–T* paths from other studies of Franciscan eclogite are shown for comparison. Paths by Massonne (1995) are radically different than all other paths, and are difficult to reconcile with existing tectonic models

diffraction (EBSD) of SiO_2 inclusions in the garnets that record the highest pressures via equilibrium (4) confirm that they are quartz and not coesite. Although it is possible that garnet resorption could have destroyed an inclusion record of higher pressures, garnets from less overprinted samples do show evidence of resorption and do not preserve such a record (Fig. 4). After the hiatus in garnet growth, phengite and clinopyroxene inclusions in the rims of garnet record similar conditions to the matrix assemblages of 10–14 kbar in the range of 350–450°C (WM). The pressures yielded by the RT barometer for the same compositions (18–23 kbar at 400–550°C) are not consistent with late matrix albite–omphacite–quartz–garnet thermobarometry (10 kbar at 400°C). These *P–T* estimates (regardless of the calibration used) suggest a counterclockwise path as previously proposed for Franciscan high-grade rocks (Oh and Liou 1990; Wakabayashi 1990; Krogh et al. 1994, Tsujimori et al. 2006). The path follows a ‘‘hairpin’’ trajectory with similar prograde and retrograde conditions.

Discussion

The reconstruction of *P–T* paths of eclogites using inclusions in garnet has been in limited use since the inception of the method by Krogh (1982). Most of the applications of this method have employed qualitative *P–T* estimates with generalized petrogenetic grids (cf. Page et al. 2003). The use of these grids ignores the complications of variable and changing bulk rock composition, as they are based on phase transitions observed in rocks of one particular composition. The use of quantitative thermobarometry circumvents this issue by calculating the locus of a

mineral equilibrium in *P–T* space, and correcting for the observed solid solutions in the minerals of interest. However, uncertainties in this method are introduced from errors in the experimental data and the thermodynamic properties extracted from them, solution models, and uncertain or incomplete chemical analyses. The relatively new method of *P–T* estimation by pseudosection calculation suffers from a combination of the uncertainties that plague both earlier methods. As with the use of petrogenetic grids, pseudosections also require evaluation of the bulk composition of the rocks. This is a difficult task considering that a significant proportion of the elements in the eclogite are sequestered in growing garnet, pyroxene, phengite and epidote, which vary through time, and which is impossible to model in the rocks under study. Moreover, elements are clearly removed to produce the resorbed garnets, others are introduced into the rock following garnet resorption, as evidenced by spikes in Mn on garnet rims, and still others are likely removed in the same events (e.g., REE in epidote).

In the high-grade blocks hosted by the Franciscan Formation, *P–T* estimations for eclogite (Wakabayashi 1990; Oh and Liou 1990; Krogh et al. 1994) have yielded counter-clockwise paths (Fig. 10). Wakabayashi (1990) estimated eclogite stage conditions of 13 kbar using albite–pyroxene–quartz barometry and garnet–omphacite thermometry on compound omphacite–albite inclusions in garnet from hornblende eclogite from the Tiburon Peninsula, California. Examination of Wakabayashi's photomicrographs (e.g., Fig. 7) suggests to the authors that albite may be a late vein mineral. Nonetheless, his estimate of 13 kbar is at least a minimum limit. A recent reevaluation of this work making use of garnet–phengite–clinopyroxene thermobarometry and pseudosections results in a late-prograde-peak-retrograde *P–T* path with similar *P–T* to those found in this study (Tsujimori et al. 2006). Krogh et al. (1994) estimated a peak metamorphism of ~16 kbar at ~500°C in eclogite from Jenner, California, using a petrogenetic grid. In addition, a minimum *P* of 10 kbar was determined using the albite–pyroxene–quartz barometer, as well as a minimum of 13 kbar based on the Si content of phengite (Massonne and Schreyer 1987). Ravna and Terry (2004) calculated peak *P–T* conditions for the Jenner eclogite (Krogh et al. 1994) of 22 kbar at 490°C, using garnet–phengite–clinopyroxene barometry, similar peak conditions to this study. The high-grade block studied by Oh and Liou (1990) yields an almost identical path to that of Krogh et al. (1994) using the same methods (Fig. 10).

Calibration of barometers

The first application of garnet–phengite–clinopyroxene thermobarometry in California by Massonne (1995) yielded much higher *P* at similar to slightly higher *T* to existing studies (Fig. 10). Mineral compositions from Wakabayashi (1990) were processed using Massonne's calibration of the thermobarometer, shifting the peak conditions of the Tiburon eclogite to 25 kbar and 600°C. Application of the same barometer to inclusions in the cores and rims of garnet from the Junction School eclogite yielded a clockwise path in which the cores of garnet record UHP conditions of ~28 kbar at ~550°C (Fig. 10). Pressure estimates in the current study are similar to or greater than those of Massonne (1995) using the RT calibration or intermediate between existing pressure minima and those calculated by Massonne (1995) using the WM calibration. Mineral compositions reported by Massonne (1995) for the Junction School eclogite are quite similar to those found in this study, further suggesting that differing calibrations of equilibrium (4) are primarily responsible for the discrepancy in thermobarometric estimates. Recent application of the Ravna and Terry calibration of equilibrium (4) to Franciscan eclogites by Ravna and Terry (2004, Jenner) and Tsujimori et al. (2006, Tiburon) yielded pressures of 24–26 kbar. These values are similar to the late prograde pressures in this study using the WM calibration but are 6–8 kbar lower than those calculated using the RT calibration.

Experimental calibration of phengite substitution in muscovite as a barometer was investigated by Velde (1965) and subsequently by Massonne and Schreyer (1987, 1989). These experimental studies are based on unreversed experiments, and furthermore, no chemical analyses were performed on the run products. Rather, compositions were estimated using bulk X-ray diffraction data alone. Nonetheless, these experiments became the basis for the thermodynamic properties of celadonite in the data base of Holland and Powell (1990, 1998). Waters and Martin (1993) first proposed equilibrium (4) as a barometer for eclogites, and updated the calibration in 1996, which was published in Wain et al. (2001). The calibration is based on the Holland and Powell (1990) data set, but an empirical adjustment was added in recognition of potential flaws in the experimental data as well as the lack of adequate phengite mixing models. The thermodynamic model was empirically calibrated to reproduce the experimental results of Schmidt (1993) as well as several natural data sets including the stability of coesite in the Tauern Window (Waters, personal communication, 2003). Since the work of Waters and Martin (1993),

Massonne (1995) developed his own thermodynamic calibration for equilibrium (4). Additional experiments by Massonne and Szpurka (1997) have led to the development of modified thermodynamic data and mixing models for phengite (Coggon and Holland 2002) that were incorporated into the 2002 THERMOCALC database. A calibration of equilibrium (4) was developed by Ravna and Terry (2004) based exclusively on the new thermodynamic data and mixing model with no empirical correction.

The discrepancy between pressures calculated for the compositions reported in this study using the WM calibration and those determined using the fully thermodynamic calibrations of Ravna and Terry (2004) or in calculations using THERMOCALC, both with or without the new phengite mixing model by Coggon and Holland (2002). Not surprisingly, pressures calculated using the Ravna and Terry (2004) barometer are within ~1 kbar of pressures calculated using THERMOCALC and the data set upon which the RT barometer is based. Ravna and Terry (2004) noted that the WM calibration yields invariably lower pressures than their calibration, but, in most cases, only by a few kilobars. Both the WM and RT barometer calibrations are linear expressions in which pressure is a function of temperature and the equilibrium constant. The WM calibration is more sensitive to lnK than the RT calibration. At low values of lnK both calibrations are within a few kilobars of each other. For the compositions found in the Junction School eclogite the calibrations differ by ~5 kbar at 500°C and ~9 kbar at 700°C. The offset between the two calibrations for the same lnK is not sufficient to fully explain the discrepancy observed in this study, but it is responsible for ~5 kbar of the ~10 kbar difference.

The discrepancies among the different calibrations is in part controlled by garnet composition. The WM calibration is tied to the Newton and Haselton (1981) binary (Ca–Mg) mixing model for garnet. When the quaternary garnet mixing model of Ganguly et al. (1996) is used with the WM barometer for the compositions in this study pressures increase by 3–7 kbar. The combination of the garnet mixing model and the offset between the two calibrations are sufficient to explain most of the pressure discrepancy observed in this study. However, the empirical adjustment made by Waters and Martin (1993) is tied to the simplified garnet mixing model, and the application of different activity models introduces an additional inconsistency.

Although the more recent barometic calibrations benefit from additional experimental data and more complicated solution models, several lines of reasoning suggest that the WM calibration used in this paper yields more realistic pressures for the Junction School eclogite. Massonne (1995) estimated peak pressure for the Healdsburg eclogite at ~28 kbar. Application of the Ravna and Terry (2004) barometer to the most phengite-rich muscovite in this study yields a pressure of 32 kbar, as opposed to 21 kbar with the Waters and Martin calibration. Pressures of ~30 kbar at 550°C are well within the stability field for coesite, and there are ample inclusions of quartz within garnet mantles that contain the phengite and clinopyroxene inclusions upon which these pressures are based. There is no suggestion of coesite in these rocks, nor is there the classic evidence of inverted coesite such as palisade textures in quartz or clear radial fracturing in the garnet host. There is no evidence to suggest that the Junction School eclogite attained UHP other than the results from the barometer in question. In addition, the temperature reported for these rocks (~550°C) is significantly lower than the temperatures recorded in well-characterized UHP terranes (e.g., Coleman and Wang 1995). In the present study, two independent barometers were applied to the inclusion assemblages in garnet. The prograde path of the Junction School eclogite is constrained both by garnet–phengite–omphacite barometry (equilibrium 4) and by the epidote–garnet–rutile–sphene–quartz barometer (equilibrium 1). Equilibria (1) and (4) yield similar pressures throughout the prograde path of the Junction School eclogite only if the empirically calibrated WM barometer is used. Even if equilibrium (4) is recalculated assuming reduced water activity and a fully ionic mixing model for sphene, pressures would increase less than 5 kbar for the garnet core assemblage and still be more than 10 kbar lower than the pressures calculated using the RT calibration. Finally, texturally late matrix garnet–omphacite–phengite assemblages yield pressures and temperatures consistent with those from equilibrium (5) and garnet–omphacite thermometry applied to the late albite–omphacite–quartz–garnet assemblage only if the WM calibration is used.

Ravna and Terry (2004) showed that their calibration yields reasonable pressures for a large number of high and ultrahigh pressure rocks. However, they also found evidence of strongly divergent results between calibrations in some rocks. Application of the RT calibration to compositions from the Carswell et al. (1997) study of Dabie eclogites (which used the WM calibration) results in a 1–13 kbar increase in pressures. Ravna and Terry (2004) also attributed this shift to a combination of garnet mixing model and barometer calibration. It is clear that the WM calibration is based on outdated thermodynamic models, and should not be, *a priori*, the calibration of choice for this barome-

ter. However, independent barometry suggests that the thermodynamically dated but empirically corrected WM calibration (Wain et al. 2001) yields more reasonable pressures for this rock than does the calibration of Ravna and Terry (2004). This points to an underlying flaw in the thermodynamic data that form the basis of the barometer. In particular, the acceptance of unreversed and unanalyzed experiments on phengite reactions by Massonne and Schreyer (1987) in the calibration of garnet–phengite–clinopyroxene barometry should be reconsidered (Essene 1989). Until the underlying thermodynamic issues are resolved, it is recommended that both empirical and thermodynamic calibrations of this barometer be used, and, where possible, supplemented by other barometry.

Tectonic implications

The *P–T* path in this study is counterclockwise, similar to many previous paths calculated for Franciscan eclogites (Oh and Liou 1990; Wakabayashi 1990; Krogh et al. 1994), but differs from them in several important points (Fig. 10). The estimates of this study yield peak pressures ~10 kbar higher than most previous workers, but, as those estimates were minima, these new data extend, but do not contradict past results other than those of Massonne (1995). New quantitative thermobarometry by Ravna and Terry (2004) and Tsujimori et al. (2006) are quite similar to those in this study. The Junction School eclogite appears to have followed a tight loop, its retrograde path roughly parallel to and ~100°C cooler than the prograde path. This tightly recumbent path is similar to those proposed by Krogh et al. (1994), Oh and Liou (1990) but contrasts with the higher temperature portions of the prograde path proposed by Wakabayashi (1990) for an hornblende eclogite from the Tiburon Peninsula. The revised *P–T* path calculated by Tsujimori et al. (2006) for the Tiburon eclogite is almost identical to the one in this study. All paths (other than those by Massonne 1995) converge at ~10 kbar and 350°C, the nearly ubiquitous blueschist facies overprint on Franciscan blocks (e.g., Moore 1984). This blueschist facies stage is nearly coincident with the estimated peak *P–T* of metamorphism for the coherent regional blueschists (e.g., Ernst 1988 and references therein).

Tectonic models of the Franciscan Formation have long struggled to explain the presence of high-grade blocks within the lower-grade Franciscan metagreywacke. Ernst (1988) subdivided blueschist and eclogite terranes into the high-temperature, collisional, Alpine type, characterized by near isothermal decompression and extensive greenschist-facies (also amphibolite- and granulite-facies) retrogression, and the low-temperature Franciscan-type, characterized by a retrograde path that retraces the prograde preserving the high *P/T* mineralogy (e.g., aragonite). Prolonged and relatively rapid subduction is invoked to maintain the depressed thermal gradients required to preserve high *P/T* conditions (Peacock 1987). However, the presence of garnet hornblendite high-grade blocks in the Franciscan, and the migmatitic kyanite amphibolite of Santa Catalina Island record a lower P/T gradient for their formation than other Franciscan rocks. A current, widely accepted model is that the hornblendite blocks were formed during the initiation of subduction along the hot lithospheric mantle hanging-wall of the early subduction zone (Platt 1975; Cloos 1985, 1986; Peacock 1987). Hornblendite blocks were then emplaced in the Franciscan sediments by a variety of routes including exhumation in a flowing mélange (Cloos 1985, 1986) or listric normal faulting in the accretionary wedge due to tectonic underplating (Platt 1986). Wakabayashi (1990) suggested that the counterclockwise path of the Tiburon hornblende eclogite was a result of the cooling of the hanging wall and its accreted metamorphic rocks as subduction progressed. The petrologic work done on Franciscan high-grade blocks in the late 1980s cemented the concepts of counter-clockwise *P–T* paths and the progression from amphibolite to eclogite to blueschist in high-grade blocks. This progression, which has been documented at several Franciscan locales (Essene and Fyfe 1967; Moore 1984; Wakabayashi 1990), has been broadly applied to all Franciscan high-grade blocks in tectonic models (Wakabayashi 1999; Anczkiewicz et al. 2004). More recently, Tsujimori et al. (2006) have revised this model, producing a hairpin *P–T* path for the Tiburon eclogite consistent with a cool prograde history.

More recent *P–T* paths of Franciscan eclogites and blueschists (Oh and Liou 1990; Krogh et al. 1994; Tsujimori et al. 2006; this study) are similar in many ways to the in situ Franciscan path (as opposed to the paths of hornblende-bearing blocks) compiled by Ernst (1988). The retrograde paths retrace the prograde paths, and the slopes of these paths require a *P/T* gradient similar to that of the Franciscan country rocks (Oh and Liou 1990; Krogh et al. 1994) or an even higher *P/T* ratio (Tsujimori et al. 2006; this study). This *P–T* topology suggests that eclogite and blueschist blocks from Healdsburg, Jenner, Ward Creek, and Tiburon may have formed in a subduction zone setting with thermal gradients comparable to or cooler than those of the Franciscan host metagreywackes. Hornblendite with late omphacite (Moore and Blake 1989)

with gently folded *P–T* paths may be relicts of a hot, early subduction zone, but other eclogite and blueschist blocks are likely the products of later subduction, and were mixed with the hornblendite blocks during exhumation. This possibility may be supported by chronologic data.

Anczkiewicz et al. (2004) reported a series of Lu–Hf isochrons for Franciscan high-grade blocks in which age decreases with temperature. The oldest ages from the blocks come from hornblendite, followed by eclogite and blueschist. The authors interpreted these data to represent a slow start to Franciscan subduction on the assumption that all of the blocks must have formed during the inception of subduction. Another interpretation of the data is that high-grade blocks were sampled throughout Franciscan subduction, and that the change from hornblendite to eclogite to garnet blueschist represents the diachronous heating, cooling and maturation of different portions of the subduction zone. There is no reason to presume that *P–T* paths of different blocks from different locales are directly related to each other, as was implicitly assumed by Anczkiewicz et al. (2004). Even adjacent high-grade blocks may record different *P–T* histories rather than being linked along a single *P–T–t* path. A coherent model will be speculative until detailed chronological information can be tied to the growth of the garnet in each assemblage.

Acknowledgments This work was supported by grant EAR 00-87448 from the National Science Foundation to EJE and SBM and by a Sigma Xi Grant-in-aid of research, and the Turner Fund of the Department of Geological Sciences at the University of Michigan to FZP. S. Passelaqua and J. Polidora generously allowed access to and sampling of the Junction School eclogite. We are endebted to C. E. Henderson for assistance with the electron microprobe and SEM. M. Manon is gratefully acknowledged for assistance in thermobarometric calculations. The electron microprobe used in this work was acquired under EAR 99-11352, and the scanning electron microscope under EAR 96-28196 from the National Science Foundation.

References

Ahn JH, Peacor DR, Essene EJ (1985) Coexisting paragonite–phengite in blueschist eclogite: a TEM study. Am Mineral 70:1193–1204

Anczkiewicz R, Platt JP, Thirlwall MF, Wakabayashi J (2004) Franciscan subduction off to a slow start: evidence from high-precision Lu–Hf garnet ages on high grade-blocks. Earth Planet Sci Lett 225:147–161

Armstrong LS, Page FZ, Essene EJ (2004) Two generations of sphene in one garnet from a Franciscan eclogite, Healdsburg, California. Geol Soc Am Abstr Prog 36:135

Bailey EH, Irwin WP, Jones DL (1964) Franciscan and related rocks, and their significance in the geology of western California. Calif Div Mines Bull 183:177

Becker GF (1888) Geology of the quicksilver deposits of the Pacific Slope. US Geol Surv Monogr 13:486

Bloxam TW (1959) Glaucophane-schists and associated rocks near Valley Ford, California. Am J Sci 257:95–112

Borg IY (1956) Glaucophane schists and eclogites near Healdsburg, California. Geol Soc Am Bull 67:1563–1583

Brothers RN (1954) Glaucophane schists from the North Berkeley Hills, California. Am J Sci 252:614–626

Carswell DA (1990) Eclogite Facies Rocks. Blackie and Son, Glasgow, p 396

Carswell DA, O'Brien PJ, Wilson RN, Zhai M (1997) Thermobarometry of phengite-bearing eclogites in the Dabie Mountains of central China. J Metam Geol 15:239–252

Catlos EJ, Sorensen SS (2003) Phengite-based chronology of K- and Ba-rich fluid flow in two paleosubduction zones. Science 299:92–95

Cloos M (1985) Thermal evolution of convergent plate margins: thermal modeling and reevaluation of isotopic Ar-ages for blueschists in the Franciscan Complex of California. Tectonics 4:421–433

Cloos M (1986) Blueschists in the Franciscan Complex of California: petrotectonic constraints on uplift mechanisms. Geol Soc Am Mem 164:77–93

Coggon R, Holland TJB (2002) Mixing properties of phengitic micas and revised garnet–phengite thermobarometers. J Metam Geol 20:683–696

Coleman RG (1980) Tectonic inclusions in serpentinites. Arch Sci 33:89–102

Coleman RG, Lanphere MA (1971) Distribution and age of high-grade blueschists, associated eclogites and amphibolites from Oregon and California. Geol Soc Am Bull 82:2397–2412

Coleman RG, Wang X (1995) Overview of the geology and tectonics of UHPM. In: Coleman RG, Wang X (eds) Ultrahigh pressure metamorphism. Cambridge University Press, Cambridge

Coleman RG, Lee DE, Beatty LB, Brannock WW (1965) Eclogites and eclogites: their differences and similarities. Geol Soc Am Bull 76:483–508

Dudley PP (1969) Electron microprobe analyses of garnet in glaucophane schists and associated eclogites. Am Mineral 54:1139–1150

Ernst WG (1988) Tectonic history of subduction zones inferred from retrograde blueschist *P–T* paths. Geology 16:1081–1084

Ernst WG, Seki Y, Onuki H, Gilbert MC (1970) Comparative study of low-grade metamorphisms in the California Coast Ranges and the outer metamorphic belt of Japan. Geol Soc Am Mem 124:276

Essene EJ (1967) Petrogenesis of Franciscan metamorphic rocks. Ph.D. thesis, University of California, Berkeley, 225 p

Essene EJ (1982) Geologic thermometry and barometry. In: Ferry JM (ed) Characterization of metamorphism through mineral equilibria. Reviews in mineralogy, vol 10. Mineralogical Society of America, pp 153–206

Essene EJ (1989) The current status of thermobarometry in metamorphic rocks. In: Daly JS, Cliff RA, Yardley BWD (eds) Evolution of metamorphic belts. Geological Society of London, London, pp 1–44

Essene EJ, Fyfe WS (1967) Omphacite in Californian metamorphic rocks. Contrib Mineral Petrol 15:1–23

Essene EJ, Fyfe WS, Turner FJ (1965) Petrogenesis of Franciscan glaucophane schists and associated metamorphic rocks, California. Beit Mineral Petrol 11:695–704

Ganguly J, Cheng W, Tirone M (1996) Thermodynamics of aluminosilicate garnet solid solution: new experimental

data, an optimized model, and thermometry applications. Contrib Mineral Petrol 126:137–151
Gealey WK (1951) Geology of the Healdsburg Quadrangle, California. In: Calif Div Mines Bull 161:7–50
Giorgetti G, Tropper P, Essene EJ, Peacor DR (2000) Characterization of non-equilibrium and equilibrium occurrences of paragonite/muscovite intergrowths in an eclogite from the Sesia-Lanzo Zone (Western Alps, Italy). Contrib Mineral Petrol 138:326–336
Graeser S, Hetherington C, Giere R (2003) Ganterite, a new barium-dominant analogue of muscovite from the Berisal Complex, Simplon Region, Switzerland. Can Mineral 41:1271–1280
Hermes OD (1973) Paragenetic relationships in an amphibolitic tectonic block in the Franciscan Terrain, Panoche Pass, California. J Petrol 14:1–32
Holland TJB (1980) The reaction albite = jadeite + quartz determined experimentally in the range 600–1,200°C. Am Mineral 65:129–134
Holland TJB (1990) Activities of components in omphacitic solid solutions: an application of Landau theory to mixtures. Contrib Mineral Petrol 105:446–453
Holland TJB, Powell R (1990) An enlarged and updated internally consistent thermodynamic dataset with uncertainties and correlations; the system K_2O–Na_2O–CaO–MgO–MnO–FeO–Fe_2O_3– Al_2O_3–TiO_2–SiO_2–C-H_2– O_2. J Metam Geol 8:89–124
Holland TJB, Powell R (1998) An internally consistent thermodynamic data set for phases of petrological interest. J Metam Geol 16:309–343
Holway RS (1904) Eclogites in California. J Geol 12:344–358
Krogh EJ (1982) Metamorphic evolution of Norwegian country-rock eclogites, as deduced from mineral inclusions and compositional zoning in garnets. Lithos 15:305–321
Krogh EJ, Oh CW, Liou JG (1994) Polyphase and anticlockwise *P–T* evolution for Franciscan eclogites and blueschists from Jenner, California, USA. J Metam Geol 12:121–134
Lanphere MA, Blake MC Jr, Irwin WP (1978) Early Cretaceous metamorphic age of the South Fork Mountain Schist in the northern Coast Ranges of California. Am J Sci 278:798–815
Li G, Peacor DR, Coombs D, Kawachi Y (1997) Solid solution in the celadonite family: the new minerals ferroceladonite, $K_2Fe^{2+}{}_2Fe^{3+}{}_2Si_8O_{20}(OH)_4$, and ferroaluminoceladonite, $K_2Fe^{2+}{}_2Al_2Si_8O_{20}$ $(OH)_4$. Am Mineral 82:503–511
Liou JG, Zhang RY, Ernst WG, Rumble D, III, Maruyama S (1998) High-pressure minerals from deeply subducted metamorphic rocks. In: Hemley RJ (ed) Ultrahigh-pressure mineralogy: physics and chemistry of the Earth's deep interior, Reviews in mineralogy and geochemistry, vol 37. Mineralogical Society of America, Washington, DC, United States, pp 33–96
Manning CE, Bohlen SR (1991) The reaction titanite + kyanite = anorthite + rutile and titanite-rutile barometry in eclogites. Contrib Mineral Petrol 109:1–9
Manon MR, Essene EJ (2005) Thermobarometry of sphene-bearing reactions: calculations with new thermodynamic data. Eos 86:V13E-0584
Manon MR, Dachs E, Essene EJ (2006) Low T heat capacity measurements and new entropy data for sphene (titanite): implications for thermobarometry of high pressure rocks. Contrib Mineral Petrol (in review)
Massonne H-J (1995) Experimental and petrogenetic study of UHPM. In: Coleman RG, Wang X (eds) Ultrahigh pressure metamorphism. Cambridge University Press, Cambridge, pp 33–95
Massonne H-J, Schreyer W (1987) Phengite geobarometry based on the limiting assemblage with K-feldspar, phlogopite, and quartz. Contrib Mineral Petrol 96:212–224
Massonne H-J, Schreyer W (1989) Stability field of the high-pressure assemblage, talc + phengite and two new phengite barometers. Eur J Mineral 1:391–410
Massonne H-J, Szpurka Z (1997) Thermodynamic properties of white micas on the basis of high-pressure experiments in the systems K_2O–MgO–Al_2O_3– SiO_2–H_2O and K_2O–FeO–Al_2O_3– SiO_2–H_2O. Lithos 41:229–250
Moore DE (1984) Metamorphic history of a high-grade blueschist exotic block from the Franciscan Complex, California. J Petrol 25:126–150
Moore DE, Blake MC, Jr. (1989) New evidence for polyphase metamorphism of glaucophane schist and eclogite exotic blocks in the Franciscan Complex, California and Oregon. J Metam Geol 7:211–228
Newton RC (1966) Some calc-silicate equilibrium relations. Am J Sci 264:204–222
Newton RC, Haselton HT (1981) Thermodynamics of the garnet-plagioclase-Al_2SiO_5-quartz geobarometer. In: Newton RC, Navrotsky A, Wood BJ (eds) Thermodynamics of minerals and melts. Springer, Berlin Heidelberg New York, pp 131–147
Nowlan EU, Schertl HP, Schreyer W (2000) Garnet-omphacite-phengite thermobarometry of eclogites from the coesite-bearing unit of the southern Dora-Maira Massif, Western Alps. Lithos 52:197–214
Nutter EH, Barber WB (1902) On some glaucophane and associated schists in the coast ranges of California. J Geol 10:738–744
Oh CW, Liou JG (1990) Metamorphic evolution of two different eclogites in the Franciscan Complex, California, USA. Lithos 25:41–53
Page FZ, Essene EJ, Mukasa SB (2003) Prograde and retrograde history of eclogites from the eastern Blue Ridge, North Carolina, USA. J Metam Geol 21:685–698
Page FZ, Essene EJ, Mukasa SB (2005) Quartz exsolution in clinopyroxene is not proof of ultrahigh pressures: evidence from eclogites from the Eastern Blue Ridge, Southern Appalachians, USA. Am Mineral 90:1092–1099
Palache C (1894) On a rock from the vicinity of Berkeley containing a new soda amphibole. Univ Cal Pub Geol Sci 1:181–192
Peacock SM (1987) Creation and preservation of subduction-related inverted metamorphic gradients. Jour Geophys Res B 92:12,763–12,781
Perkins D, III, Westrum EF Jr, Essene EJ (1980) The thermodynamic properties and phase relations of some minerals in the system CaO–Al_2O_3–SiO_2– H_2O. Geochim Cosmochim Acta 44:61–84
Platt JP (1975) Metamorphic and deformational processes in the Franciscan Complex, California: some insights from the Catalina Schist terrane. Geol Soc Am Bull 86:1337–1347
Platt JP (1986) Dynamics of orogenic wedges and the uplift of high-pressure metamorphic rocks. Geol Soc Am Bull 97:1037–1053
Proyer A, Dachs E, McCammon C (2004) Pitfalls in geothermobarometry of eclogites: Fe^{3+} and changes in the mineral chemistry of omphacite at ultrahigh pressures. Contrib Mineral Petrol 147:305–318
Ransome FL (1894) The geology of Angel Island (California). Univ Cal Pub Geol Sci 1:193–234
Ransome FL (1895) On lawsonite, a new rock-forming mineral from the Tiburon Peninsula, Marin County, California. Univ Cal Pub Geol Sci 1:301–312

Ravna EJK (2000) The garnet-clinopyroxene Fe^{2+}-Mg geothermometer: an updated calibration. J Metam Geol 18:211–219

Ravna EJK, Paquin J (2003) Thermobarometric methodologies applicable to eclogites and garnet ultrabasites. In: Carswell DA, Compagnoni R (eds) EMU notes in mineralogy, vol 5. Ultrahigh pressure metamorphism. pp 1–34

Ravna EJK, Terry MP (2004) Geothermobarometry of UHP and HP eclogites and schists—an evaluation of equilibria among garnet–clinopyroxene–kyanite–phengite–coesite/quartz. J Metam Geol 22:579–592

Ross JA, Sharp WD (1988) The effects of sub-blocking temperature metamorphism on the K/Ar systematics of hornblendes: $^{40}Ar/^{39}Ar$ dating of polymetamorphic garnet amphibolite from the Franciscan Complex, California. Contrib Mineral Petrol 100:213–221

Schmidt MW (1993) Phase relations and compositions in tonalite as a function of pressure: an experimental study at 650°C. Am J Sci 293:1011–1060

Sharp WD, Ross JA, Dickinson WR (1987) Are high-grade ''knockers'' in accretionary wedges samples of forearc basement? Evidence from the Franciscan Complex, California. Geol Soc Am Abstr Prog 19:840

Sharp ZD, Essene EJ, Smyth JR (1992) Ultra-high temperatures from oxygen isotope thermometry on a coesite-sanidine grospydite. Contr Mineral Petrol 112:358–370

Shau YH, Feather ME, Essene EJ, Peacor DR (1991) Genesis and solvus relations of submicroscopically intergrown paragonite and phengite in a blueschist from California. Contrib Mineral Petrol 106:367–378

Sorensen SS, Grossman JN, Perfit MR (1997) Phengite-hosted LILE enrichment in eclogite and related rocks; implications for fluid-mediated mass transfer in subduction zones and arc magma genesis. J Petrol 38:3–34

Switzer GS (1945) Eclogite from the California glaucophane schists. Am J Sci 243:1–8

Tropper P, Essene EJ, Sharp ZD, Hunziker, JC (1999) New pressure constraints in high pressure rocks: applications of K-feldspar–jadeite–quartz barometry to eclogite facies metagranites and metapelites in the Western Alps. J Metam Geol 17:195–209

Tropper P, Manning CE, Essene EJ (2002) The substitution of Al and F in titanite at high pressure and temperature: experimental constraints on phase relations and solid solution properties. J Petrol 43:1787–1814

Tropper P, Manning CE, Essene EJ (2006) Constraints on titanite activity in the system $CaTiSiO_4O$–$CaAlSiO_4F$ and the use of titanite solid solutions for thermobarometry in metamorphic rocks. Eos, Trans AGU 87:V31B–0577

Tsujimori T, Matsumoto K, Wakabayashi J, Liou J (2006) Franciscan eclogite revisited: reevaluation of *P–T* evolution of tectonic blocks from Tiburon Peninsula, California. Min Pet 88:243–267

Velde B (1965) Phengite micas; synthesis, stability, and natural occurrence. Am J Sci 263:886–913

Wain AL, Waters DJ, Austrheim H (2001) Metastability of granulites and processes of eclogitisation in the UHP region of western Norway. J Metam Geol 19:607–623

Wakabayashi J (1990) Counterclockwise *P–T–t* paths from amphibolites, Franciscan Complex, California: relics from the early stages of subduction zone metamorphism. J Geol 98:657–680

Wakabayashi J (1999) The Franciscan: California's classic subduction complex. Geol Soc Am Spec Pap 338:111–121

Wakabayashi J, Deino A (1989) Laser-probe $^{40}Ar/^{39}Ar$ ages from high grade blocks and coherent blueschists, Franciscan Complex, California: preliminary results and implications for Franciscan tectonics. Geol Soc Am Abstr Prog 21:267

Wang L, Essene EJ, Zhang Y (1999) Mineral inclusions in pyrope crystals from Garnet Ridge, Arizona, USA: implications for processes in the upper mantle. Contrib Mineral Petrol 135:164–178

Waters DJ, Martin HN (1993) Geobarometry in phengite-bearing eclogites. Terra Abstr 5(Suppl 1):410–411